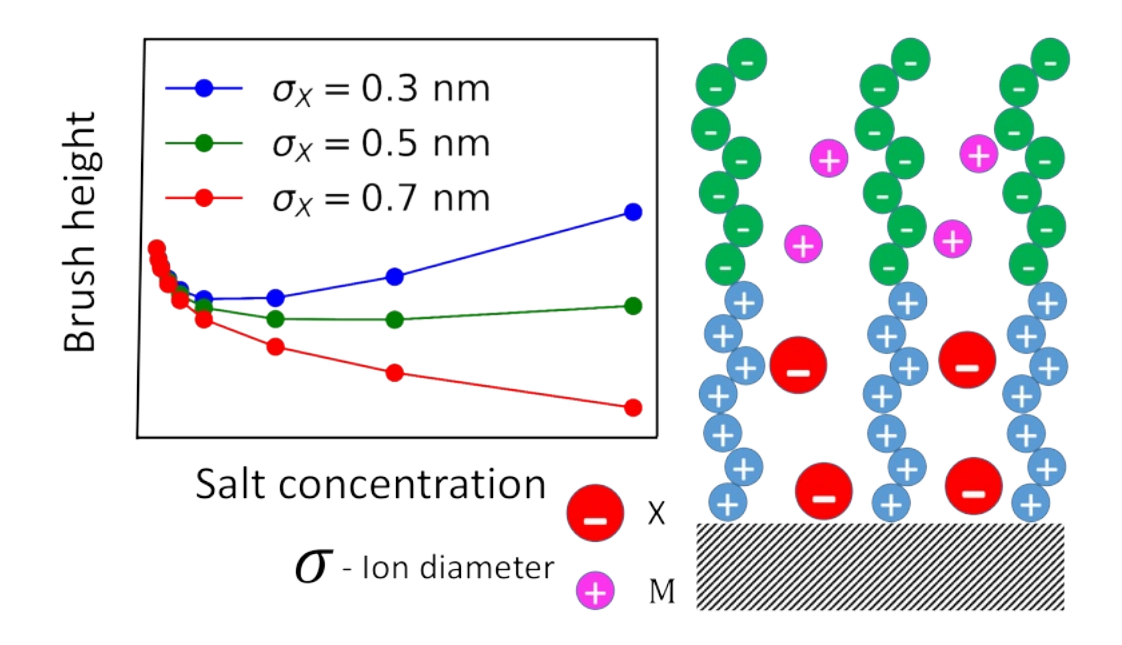
# Modeling ionic and sequence effects on the swelling behavior of polyampholyte brushes

Debadutta Prusty,† Alejandro Gallegos,‡ and Jianzhong Wu\*,†

†Department of Chemical and Environmental Engineering, University of California, Riverside, California 92507, USA

‡Division of Chemistry and Chemical Engineering, California Institute of Technology,
Pasadena, California 91125, USA

E-mail: jwu@engr.ucr.edu



#### Abstract

The structural responses of polyampholytes to various chemical stimuli are sensitive to the sequence of monomeric groups that bear positive and negative charges. However, a theoretical understanding is yet to be established to account for the sequence effects under diverse environmental conditions such as solution pH, salt concentration, and ion valence. As a first step towards delineating the underlying physics, in this work, we consider strong polyampholyte brushes with either a diblock or an alternating chain architecture and study their structure and swelling behavior in response to variations in salt concentration, ion size and valency using a polymer density functional theory. As the salt concentration increases, an alternating brush displays a re-entrance behavior, characterized by an initial reduction of the brush height followed by a subsequent brush expansion. The ion size effects become appreciable only at high salt concentrations, wherein a reduction of the ion size leads to an increased brush height. For a diblock brush, however, the brush height decreases monotonically with the addition of salt when the counterions to the lower block are significantly larger than the polymer segments. A re-entrance behavior is observed only when the ion diameter is equal to or smaller than that of the monomers. The non-monotonic trend contradicts the so-called antipolyelectrolyte effect, which predicts an expansion of the polyampholyte brush upon the addition of salt. While the variation of the counterion size for the upper block generates a similar swelling behavior, the ion size has opposite effects on the degree of interblock association. These trends have been rationalized by considering the interplay of excluded-volume interactions with electrostatic and correlation effects. For both types of polyampholyte brushes, the salt effects become significantly more pronounced in the presence of divalent ions, with the alternating brush displaying a stronger dependence on the salt concentration.

#### 1. Introduction

Polymers containing both positive and negative charges on their backbones, known as polyampholytes, are being actively pursued in soft-matter research <sup>1–3</sup> owing to their usefulness in applications such as oil recovery <sup>4</sup> and drag reduction. <sup>5</sup> The presence of intra-chain electrostatic attraction and repulsion endows unique properties to polyampholytes, differ-

ent from their homopolyelectrolyte counterparts in solutions, <sup>1,6</sup> in their gel forms, <sup>7</sup> and at interfaces. <sup>8,9</sup> A well-known example is the so-called anti-polyelectrolyte effect, which refers to the expansion of polyampholyte chains with equal or near equal amounts of positive and negative charges in solutions <sup>10</sup> or gels <sup>11</sup> upon salt addition as opposed to a collapse of the polymer structure seen in homo-polyelectrolyte systems. The equal amounts of positive and negative charges and the resulting charge neutrality therefrom make the structure of polyampholytes relatively insensitive to interaction with external species, <sup>12</sup> which renders polyampholyte brushes better anti-fouling resistance against proteins, bacteria and cells than single-component polymers. <sup>13</sup> Studies on the sliding behavior of zwitterionic brushes have demonstrated that they exhibit a lower friction coefficient compared to conventional polyelectrolyte brushes, making them extremely desirable for anti-friction applications. <sup>14,15</sup> Previous research also revealed that weak polyampholytes exhibit simultaneous up regulation and down regulation of acidic and basic monomers upon the addition of salt, a phenomenon in stark contrast with the charging behavior of a single-component weak polyelectrolyte brush. <sup>9</sup>

Polyampholytes can be classified into two major categories in terms of the backbone architecture: i) those carrying positively and negatively charged units on separate monomers; and ii) those containing both a positively charged unit and a negatively charged unit in the same monomer. Examples for the first category of polyampholytes include 2-(dimethylamino)ethyl methacrylate-methacrylic acid block copolymer (DMAEMA-MAA). Polyampholytes such as poly(sulfobetaine methacrylate) (PSBMA), poly(carboxybetaine methacrylate) (PCBMA), and poly(2-methacryloyloxyethyl phosphorylcholine) (PMPC), <sup>16,17</sup> belong to the second category. The latter type of polyampholytes is often referred to as zwitterionic polymers.

Both types of polyampholytes display rich phase behavior in solutions as well as on surfaces. An important factor dictating their phase behavior is the identity of salt ions. Distinctive anion effects were experimentally observed on the conformation of zwitterionic polymers in response to the ionic strength of NaX solutions, where  $X = SO_4^{2-}$ ,  $Cl^-$ ,  $Br^-$ ,  $NO_3^-$ ,  $ClO_4^-$  and  $SCN^-$ . Among non-zwitterionic polyampholytes, another important pa-

rameter dictating the structural behavior is the chain architecture. Experimental studies on synthetic polyampholytes of L-glutamic acid (E) and L-lysine (K) revealed a positive correlation between the blockiness of charged groups and coacervation ability. <sup>19</sup> Theoretical investigations of diblock, alternating, and random polyampholytes found that the propensity for phase separation was maximized for polymers with the diblock sequence and the lowest for those with alternating sequence. <sup>20,21</sup> For brush systems, existing experimental efforts have mostly focused on zwitterionic brushes and their structural response to different salt species. Ellipsometry and X-ray reflectivity (XRR) measurements indicate that the swelling behavior of poly(cysteine methacrylate) (PCysMA) brushes is sensitive to the identity of both cations and anions. 8 The brush swelling was attributed to the dissociation of cationic and anionic monomers, and the brush shrinkage is due to strong chelation between multivalent cations and negatively charged monomers. The specific anion effect on brush swelling followed the Hofmeister series, suggesting the important role of ion hydration. Xiao and coworkers synthesized different zwitterionic brushes with various cationic groups such as imidazolium, ammonium, and pyridinium and with different carbon spacer lengths between the positively charged and the negatively charged monomers. <sup>22</sup> Ellipsometry and atomic force microscopy (AFM) measurements indicate that reducing the spacer length enhances the antipolyelectrolyte effect.

The influence of various physicochemical parameters on the structural properties of polyampholyte brushes has been reported by a number of theoretical and simulation studies. Molecular modeling offers a valuable tool for understanding the essential physics without facing significant challenges related to the synthesis of complex polymer systems and the characterization of microscopic structures under different experimental conditions. Using all-atom molecular dynamics (MD) simulation, Li et al.<sup>23</sup> studied the interfacial behavior of zwitterionic peptides consisting of repeating units of lysine and glutamic acid in different sequences. The simulation results indicate that, under salt-free conditions, an alternating architecture shows the best anti-fouling performance. The addition of divalent cations would

lead to dehydration of the peptides and inter-linkage between glutamic acid monomers. Zhu et al. $^{24}$  compared the self-cleaning ability of polyanionic and polyzwitterionic brushes in crude oil using MD simulation and a coarse-grained model. These authors predicted that, at low grafting densities, polyzwitterions are able to form an intermolecular cross-linked network, resulting in better oil repellancy. However, at high grafting densities, polyanions exhibit better performance due to the formation of polymer bundles via hydrophobic interactions. Based on a lattice mean-field theory, Susharina and Linse<sup>25</sup> investigated the structure of strong diblock polyampholyte brushes and found the two blocks to be in an overlapping configuration in the limit of zero salt concentration. Upon the addition of salt, the lower block underwent compression, separated from the extended upper block. Borowko et al. $^{26}$ studied ion adsorption in polyampholyte brushes with diblock, alternating, and intermediate architectures using a classical density functional theory (cDFT). The ion selectivity with respect to cation and anion absorption into the brush was found lowest for the brush with an alternating structure. The polyampholyte brushes exhibit sequence-dependent responses to salt addition, with a shrinkage of the polymer structure observed for the alternating architecture and an expansion for the diblock architecture. Similar brush systems were investigated with coarse-grained MD simulations.<sup>27</sup> Variations in monomeric sequence, counterion valency, and the rigidity of polymer chains unveiled maximally collapsed structures for brushes with flexible diblock configurations and a brush expansion when one of the blocks was rigid. The simulation results suggested that counterion valency effect was significant only when one of the blocks was rigid. Additional efforts have been reported focusing on weak polyampholyte brushes and how external stimuli affect their structural behavior. Prusty et al.<sup>9</sup> used a molecular theory to study the dissociation of acid and base monomers in diblock polyampholyte brushes and observed brush swelling with an increase in salt concentration, accompanied by a reduction in association in one block and an increase in association in the other. The molecular theory treats electrostatic correlations at the mean-field level, which misses correlation effects. MD simulation carried out by Yuan et al. 28 indicated that polyampholytes with a diblock structure are more responsive to pH compared to those with alternating sequences. The ionization of polyampholytes was found relatively insensitive to the grafting density. Qualitatively, these findings are in good agreement with the general trends reported by Prusty et al. As was noted before, ion specificity can play an important role but to our knowledge, there have been no theoretical studies concerning the specific ion effects on zwitterionic brushes. Page 29,30 Specific ion effects arise from multiple factors such as a) hydrated ion size, and by ion shape, c) charge density and charge distribution within the ion, d) presence of hydrophobic groups in the ion, and e) the interaction between hydration layer of ion and that of monomers. While capturing the effects of all the above-mentioned parameters requires quantum mechanical simulations, ion size effects can be conveniently studied through cDFT by assuming the hydrated ions to be charged hard spheres. In our recent work on opposing polyelectrolyte brushes, we found that increasing the counterion size reduced brush-brush adhesion. Hence, notwithstanding its simplicity, we believe a cDFT study can help us obtain qualitative insights into the effect of various cations and anions on polyampholyte systems with different backbone architectures.

In this work, we explore the structure and swelling behavior of strong polyampholyte brushes at different salt concentrations and the diameters of cations and anions using a coarse-grained model and cDFT. We restrict ourselves to non-zwitterionic brushes owing to the ease of modelling. Each brush consists of diblock or alternating polyampholytes with the cationic end grafted to a planar substrate. To our knowledge, there are no previous reports on the theoretical or experimental studies of specific salt ion effects on non-zwitterionic polyampholyte brushes. However, due to the close proximity between positively charged and negatively charged monomers in the alternating architecture, we expect a qualitative match between the theoretical results and experimental observation of similar effects on zwitterionic brushes.

The remainder of this article is organized as follows. In the next section, we describe briefly the theoretical model, which is similar to that used in our previous work on opposing polyelectrolyte brushes.<sup>33</sup> In section 3, we present the numerical results. Specifically, section 3.1 compares the swelling behavior of a symmetric diblock brush and that of an alternating brush at low salt concentrations. In section 3.2, we analyze the changes in brush height as the salt concentration is increased. To understand the structural changes underlying the observed trends, we also examine the density profiles of monomeric species, the distributions of free ions, as well as the local charge density and local electric potential in different brush systems. Next, in section 3.3, we vary the size of counterions relative to monomers and analyze the resulting effect on the brush swelling behavior. We consider both counterions to the lower (cationic) block and counterions to the upper (anionic) block. In this section, we also contrast the results with those on the alternating brush system and discuss their connections with experimental results from the literature. In section 3.4, we explore the ion size effects at different valencies of the counterions to the upper block. Finally, in section 4, we present conclusions along with a few possible future directions for the extension of the current work.

## 2. Molecular Model and Theory

The molecular model used in the current work is similar to those used in our previous publications on polyelectrolyte brushes.  $^{34,35}$  Schematically, Figure 1 presents two types of polyampholyte brushes, one with an alternating and the other with a symmetric diblock architecture. The system is in contact with a reservoir of aqueous solution at a finite salt concentration  $c_s$ . All polymer segments are assumed to carry either a positive or a negative unit charge. For the diblock polyampholyte brush, the cationic block is designated as the lower block as it is tethered to the substrate; the anionic block is referred to as the upper block and is freely extended to the aqueous solution. For the polyampholyte with an alternating architecture, the grafted segment is assigned as a cationic monomer. Throughout this work, all polymer chains have the same degree of polymerization, designated as  $N_P$ , and the grafting

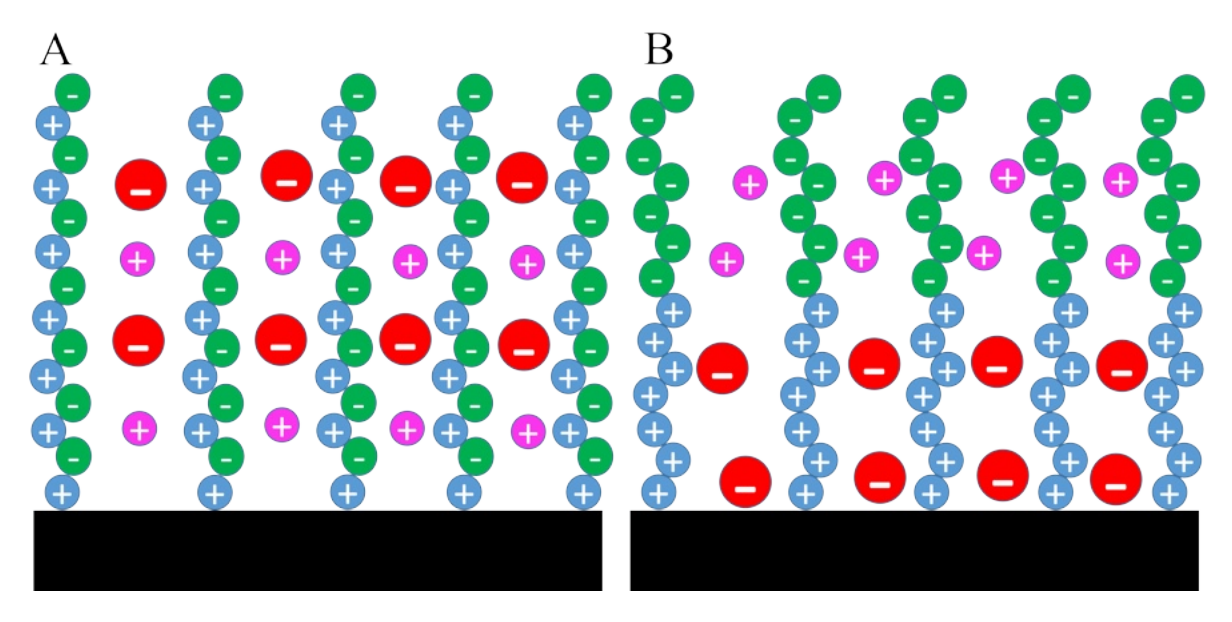


**Figure 1:** A schematic representation of the polyampholyte brush systems studied in the current work. Panel A is for the alternating architecture and panel B is for the diblock architecture. In the current representation, the anions are larger than other monomers and cations.

density of each brush is defined as  $\sigma_g = n_P/A$ , where A is the surface area of the substrate and  $n_P$  is the number of grafted chains on each surface.

We assume that the local densities of each chemical species and the electrical potential vary only in the direction perpendicular to the substrate. The assumption of lateral homogeneity is reasonable as the systems of interest in this work have high grafting density and relatively large chain length. The salt is represented by  $MX_Z$ , where  $Z = Z_+$  is the valency of counterions to the upper block (viz., away from the surface). Unless the size effects of a particular species are considered, the diameters of all monomeric species, i.e., polymer segments (P), cations (M), and monovalent anions (X), are kept equal at  $\sigma_P = 0.425$  nm. The selection of diameter is motivated by our previous works on polyelectrolyte brushes.<sup>36</sup> However, we note that several well known salt ions have diameters in the range of size considered in the study. The hydrated ion diameters of Na<sup>+</sup>, K<sup>+</sup>, Rb<sup>+</sup> and Cs<sup>+</sup> are 0.5 nm, 0.27 nm, 0.31 nm and 0.37 nm, respectively. As for anions, the hydrated ion diameters of F<sup>-</sup>, Cl<sup>-</sup>, SCN<sup>-</sup> and ClO<sub>4</sub> are 0.24 nm, 0.42 nm, 0.25 nm and 0.27 nm, respectively.<sup>37</sup> The solvent is

represented by a continuum background with a relative dielectric constant of  $\epsilon_r = 78$ , the value for liquid water at room temperature.

The interaction among monomers and salt ions is described by a combination of the Coulomb energy and a hard-core potential as described in the primitive model of electrolyte solutions:

$$\beta u_{ij}(\mathbf{r}_{ij}) = \begin{cases} \infty, & r_{ij} < \sigma_P, \\ l_B Z_i Z_j / r_{ij}, & r_{ij} \ge \sigma_P \end{cases}$$
 (1)

where  $l_B = \beta e^2/(4\pi\epsilon_0\epsilon_r)$  is the Bjerrum length,  $Z_i$  and  $Z_j$  are ion valences,  $r_{ij} = |\mathbf{r}_{ij}|$  is the center-to-center distance between ionic species i and j, and  $\epsilon_0$  is the permittivity of free space. As usual,  $\beta = 1/(k_BT)$ , T is the temperature in kelvin, and  $k_B$  is the Boltzmann constant. While the Bjerrum length (viz., the dielectric constant) of the electrolyte solution varies with the salt concentration, the ion effect becomes most relevant at high salt concentration (larger than 1.0 M). Furthermore, it is unclear how the inhomogeneous distribution of salt ions and polymer segments impacts the solvent dielectric constant, particularly within the brush. Thus, for simplicity and to avoid confusion by introducing empirical mixing rules, we have chosen to keep the Bjerrum length constant ( $l_B \approx 0.714$  nm).

In cDFT calculations,<sup>34</sup> we minimize the grand potential for each polyampholyte brush at a specific thermodynamic condition:

$$\Omega = F - \int d\mathbf{r} \rho_M(\mathbf{r}) [\mu_M - V_M^{ext}(\mathbf{r})] - \int d\mathbf{r} \rho_X(\mathbf{r}) [\mu_X - V_X^{ext}(\mathbf{r})]$$

$$+ \int d\mathbf{R} \rho_P(\mathbf{R}) V_P^{ext}(\mathbf{R})$$
(2)

where  $\mathbf{R} = (\mathbf{r}_1, \mathbf{r}_2, \mathbf{r}_3, ..., \mathbf{r}_{N_P})$  denotes the segment positions of a single chain (i.e., the polymer configuration),  $\mu_M$  and  $\mu_X$  are the chemical potentials of cations and anions, respectively. The external potential,  $V_i^{ext}(\mathbf{r})$ , describes the hard-core interactions of species i

with the substrate and, for each monomeric species, is given by

$$\beta V_i^{ext}(\mathbf{r}) = \begin{cases} \infty, & z < \sigma_P/2 \\ 0, & \text{otherwise.} \end{cases}$$
 (3)

The intrinsic Helmholtz energy (F) can be decomposed into the ideal and excess contributions<sup>38</sup>

$$F = F_{id} + F_{ex}. (4)$$

The ideal part of the intrinsic Helmholtz energy is exactly known:

$$\beta F_{id} = \int d\mathbf{R} \rho_P(\mathbf{R}) \left\{ \ln[\rho_P(\mathbf{R})] - 1 \right\} + \int d\mathbf{R} \rho_P(\mathbf{R}) \beta V_P^b(\mathbf{R}) + \int d\mathbf{r} \rho_M(\mathbf{r}) \left\{ \ln[\rho_M(\mathbf{r})] - 1 \right\} + \int d\mathbf{r} \rho_X(\mathbf{r}) \left\{ \ln[\rho_X(\mathbf{r})] - 1 \right\}$$
(5)

The first term on the right side of Eqn.(5) is associated with the conformation of the grafted chains, the second term is related to the chain connectivity as described by the bond potential  $V_P^b(\mathbf{R})$ , and the third and fourth terms account for the translational entropies of the cations and anions, respectively. The excess part,  $F_{ex}$ , includes contributions due to the excluded volume interactions between all monomeric species, the electrostatic interactions, correlations effects due to monomer-monomer interactions and chain connectivity.<sup>39</sup> The expressions for these contributions are well known and are restated in Supporting Information (SI).

The essential task of cDFT calculations is to minimize the grand potential with respect to the density profiles of polymeric species and free ions. More explicitly, the equation for solving the polymer conformation density,  $\rho_P(\mathbf{R})$ , reads as:

$$\ln \rho_P(\mathbf{R}) = \ln K - \beta V_P^b(\mathbf{R}) - \beta \sum_{i=1}^{N_P} \lambda_i(\mathbf{r}_i) - \beta V_P^{ext}(\mathbf{R})$$
 (6)

where  $\lambda_i(\mathbf{r}) = \delta F_{ex}/\delta \rho_{iP}(\mathbf{r})$  stands for the one-body potential for segment *i* of the polymer chain, and *K* is a constant determined by normalization conditions applied to all polymer

segments, i.e.,

$$\int dz \rho_{iP}(z) = \sigma_g \tag{7}$$

with  $\rho_{iP}(z)$  being the local density of polymer segment i.<sup>35</sup> The monomer density is related to the polymer conformation density by

$$\rho_j(\mathbf{r}) = \sum_i \rho_{iP}(\mathbf{r}) = \sum_i \int d\mathbf{R} \delta(\mathbf{r} - \mathbf{r}_i) \rho_P(\mathbf{R})$$
 (8)

where subscript j = A, B denotes the monomer type, i.e., cationic (A) or anionic (B), and the summation over index i runs over all monomers of type j in each polymer chain. For a brush with a diblock architecture, the monomer density takes the form

$$\rho_{j}(\mathbf{r}) = \begin{cases} \delta(z - z_{g}) + \sum_{i} K \exp\left[-\beta \lambda_{i}(\mathbf{r})\right] G_{iP}^{L}(\mathbf{r}) G_{iP}^{R}(\mathbf{r}), & j = A\\ \sum_{i} K \exp\left[-\beta \lambda_{i}(\mathbf{r})\right] G_{iP}^{L}(\mathbf{r}) G_{iP}^{R}(\mathbf{r}), & j = B \end{cases}$$
(9)

where  $G_{iP}^L(\mathbf{r})$  and  $G_{iP}^R(\mathbf{r})$  are the propagator functions for the polymer chains, and  $\delta(z)$  represents the Dirac-delta function. In Eqn. (9), the delta function represents the contribution from the first A monomer, which is fixed at  $z_g = \sigma_P/2$ . Under the assumption of lateral homogeneity adopted in this work, the propagator functions simplify to

$$G_{iP}^{L}(z) = \int dz' \exp[-\beta \lambda_i(z')] \frac{\Theta(\sigma_P - |z - z'|)}{2\sigma_P} G_{(i-1)P}^{L}(z)$$
(10)

and

$$G_{iP}^{R}(z) = \int dz' \exp\left[-\beta \lambda_i(z')\right] \frac{\Theta(\sigma_P - |z - z'|)}{2\sigma_P} G_{(i+1)P}^{R}(z)$$
(11)

where  $G_{N_PP}^R(z) = 1$  and  $G_{2P}^L(z) = \exp[-\lambda_2(z_g)]\Theta(\sigma_P - |z - z_g|)/(2\sigma_P)$ . The boundary condition relating to the second monomer,  $G_{2P}^L(z)$ , reflects the fact that the first monomer is fixed in position  $z = \sigma_P/2$  and hence, its one body potential is equal to infinity everywhere except the grafting location. cDFT predicts that the density profiles for anions and cations

follow the modified Boltzmann equation

$$\rho_{\alpha}(z) = \rho_{\alpha}^{b} \exp\{-\beta \left[V_{\alpha}^{ext}(z) + \lambda_{\alpha}(z) - \mu_{\alpha}^{ex}\right]\}$$
(12)

where  $\mu_{\alpha}^{ex}$  is the excess chemical potential of species  $\alpha$  in the bulk solution, and  $\rho_{\alpha}^{b}$  is the ion density in the bulk.

Since the density profiles depend on the one-body potential and vice versa, the above equations are self-consistent and are solved numerically. In solving these equations, we divide the space into discrete grids in z direction and use the Picard iteration to solve the discretized equations.<sup>34</sup> The iteration stops when the difference in densities between two successive iterations becomes less than  $10^{-6}$  times the corresponding bulk densities for mobile species and when the difference in surface density ( $\int \rho_i(z)dz$ ) for any monomer is less than  $10^{-6}$  times the chain grafting density.

### 3. Results and discussion

## 3.1. Microscopic structure of polyampholyte brushes

To understand the swelling behavior of polyampholyte brushes, it is instructive to start our analysis with the lateral distributions of polymer segments and free ions. For simplicity, we assume that the electrolyte solution consists of a monovalent salt at low concentration  $(c_s = 1 \text{ mM})$ , and that the brush systems are charge symmetric other than a neutral surface, i.e., each polymer chain bears the same number of cationic and anionic monomers and all charged segments have the same size and valence. In addition to different polyampholyte types (viz., block and alternating structures), we have considered different polymer chain lengths (m=40 and 80) and tethering densities  $(\sigma_g = 0.4 \text{ and } 0.8)$ .

Figure 2 presents the density profiles of charged monomers (panel A) and salt ions (panel D) for a diblock polyampholyte brush with the cationic end grafted on a neutral surface.

Also shown in this figure are the density profiles of various polymer segments (panel B), a schematic of the polymer configuration (panel C), the local electric potential (panel E), and the local charge density near the surface (panel F). Panel A shows that, except near the grafting surface, the density profiles of cationic and anionic monomers are virtually indistinguishable, suggesting the formation of intramolecular complexes between the oppositely charged polyelectrolyte blocks at low tethering densities. Due to the tethering of one end to the surface, the cationic block exhibits a segment density profile significantly different from that of the anionic block near the surface, as indicated by the pronounced oscillatory behavior. Although the polyampholyte brush bears no net charge, the uneven distribution of cationic and anionic segments within the brush leads to a significant accumulation of anions and, subsequently, the formation of an electric double layer (EDL) beyond the brush regime (panel D). As expected, the EDL thickness is on the order of the Debye screening length ( $\sim 10$  nm), consistent with the prediction of conventional EDL theories. <sup>40</sup> Inside the polyampholyte brush, the tethering of cationic monomers leads to a strong layer of anions accumulated at the grafting surface. A weak spike is observed in the density profile of anions at the brush edge due to the uneven distributions of cationic and anionic monomers. Because of the monomer concentration is higher than that of free ions by about three orders of magnitude, a small difference in the local densities of cationic and anionic monomers have drastic effect on the ion distributions.

The self-association of cationic and anionic blocks within each polyampholyte chain is evident from the distributions of various polymer segments as shown in Figure 2B. The cationic monomers near the junction between cationic and anionic blocks  $(\bar{A}_{18-20})$  are exposed near the brush surface, as suggested by their density profiles at the brush edge. The density profiles of the three ending anionic segments  $(\bar{B}_{18-20})$  are peaked near the grafting surface due to their association with the tethered cationic segments  $(\bar{A}_{2-4})$ . Interestingly, the middle anionic monomers  $(\bar{B}_{9-11})$  are also enriched near the surface, suggesting that the upper (anionic) block is more compressed and closer to the surface than the lower (cationic)

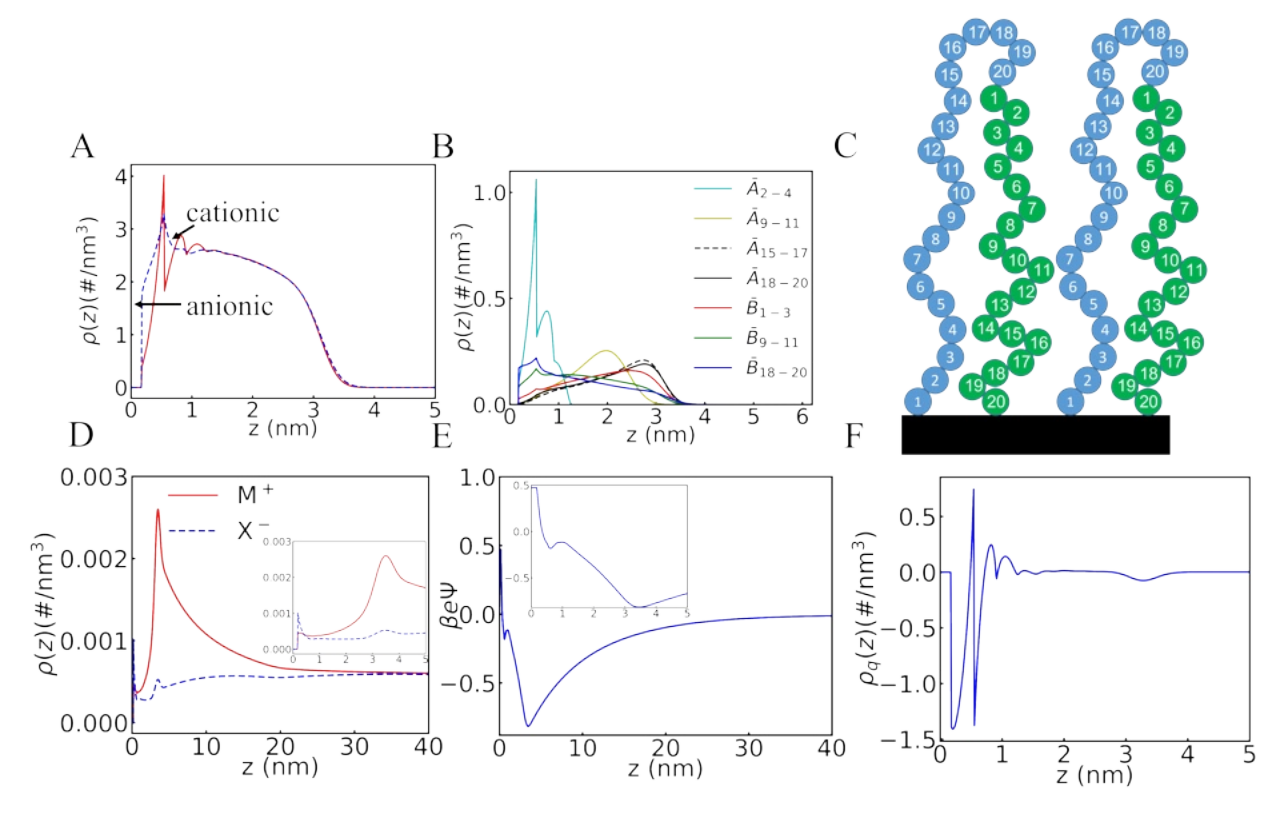


Figure 2: The microscopic structure of a diblock polyampholyte brush  $A_{20}B_{20}$  with A standing for cationic monomers and B for anionic monomers, and the cationic block grafted to a neutral surface. (A) Monomer density profiles; (B) segment density profiles averaged over 3 consecutive monomers at different locations along the polyampholyte chain; (C) schematic of the polyampholyte conformation; the blue spheres represent cationic segments, and the green spheres representing anionic segments; (D) salt ion density profiles; (E) electrical potential profile; and (F) charge density profile. Here, the grafting density is  $\sigma_g = 0.4 \text{ nm}^{-2}$ , and the salt concentration is  $c_s = 1 \text{ mM}$ .

block, as depicted schematically in Figure 2C. The encapsulation of the anionic block is also evident from the density profiles of cationic segments  $\bar{A}_{18-20}$  and  $\bar{A}_{15-17}$ , which are located furthest from the grafting surface. The significant overlap between the density profiles of these polymer segments reveals that the polymer chains start bending a few monomers before the junction between two blocks, and the density profiles flatten thereafter before the anionic segments turn towards the surface. The slight enrichment of anionic segments at the brush surface corroborates the aforementioned claim that the upper block is more compressed than the lower block. Additionally, we observe that the segment density profiles of cationic monomers are slightly narrower than the corresponding anionic monomers sym-

metric with respect to the intersection between two blocks. This can be understood from the fact that the anionic block, due to being far from the grafted (1st) monomer, is free to explore a greater number of conformations than the cationic block, which is restrained due to the constraint of chain connectivity.

Figure 2E and F present the local electric potential and net charge density near the polyampholyte brush. Except at distances immediately close to the grafting surface, the electric potential is negative throughout the brush regime. Consistent with the ionic density profiles, the electric potential extends over a distance much greater than the brush thickness, indicating an overall negative charge within the brush. The positive potential close to the surface can be attributed to the grafted cationic monomers, which cannot be fully neutralized by anionic segments and anions due their additional degrees of freedom in the solution. The local charge density near the grafting surface reflects the strong interplay of electrostatic attraction and excluded volume effects, leading to enhanced negative peaks and an oscillatory charge distribution. Compared to the monomer densities, the cation and anion densities are extremely small (approximately by a factor of 1/1000). The weak negative peak at the brush edge again signifies the slight uneven distributions of cationic and anionic polymer segments.

At moderate graft densities and low salt concentrations, the back folding of diblock polyampholyte chains are anticipated due to the strong electrostatic attraction between the oppositely charged polymer segments. Based on a lattice mean-field theory, <sup>41</sup> Shusharina and Linse demonstrated that, at low salt concentrations, the configuration of a symmetric diblock polyampholyte brush exhibits complete overlap between the two blocks. Similarly, a molecular theory study of symmetric weak polyampholyte brushes showed substantial back folding of the upper block as the salt concentration was decreased at intermediate pHs, where the degrees of dissociation are approximately identical for both types of monomers. Later, a similar study on weak polyampholyte brushes through MD simulations showed the back folding of diblock polyampholyte chains to be prominent at grafting densities below the overlap density. As shown in Figure S1 and S2, strong back folding is also observed

for diblock polyampholyte brushes at much higher grafting density and longer chain length. Because in this work all monomers have fixed charges, the electrostatic attraction overcomes the excluded volume penalty associated with the high densities of monomers in the brush in the folded conformation. The polyampholyte chains display an extended conformation only at sufficiently high grafting densities when the segment-segment interactions are dominated by the excluded volume effects.

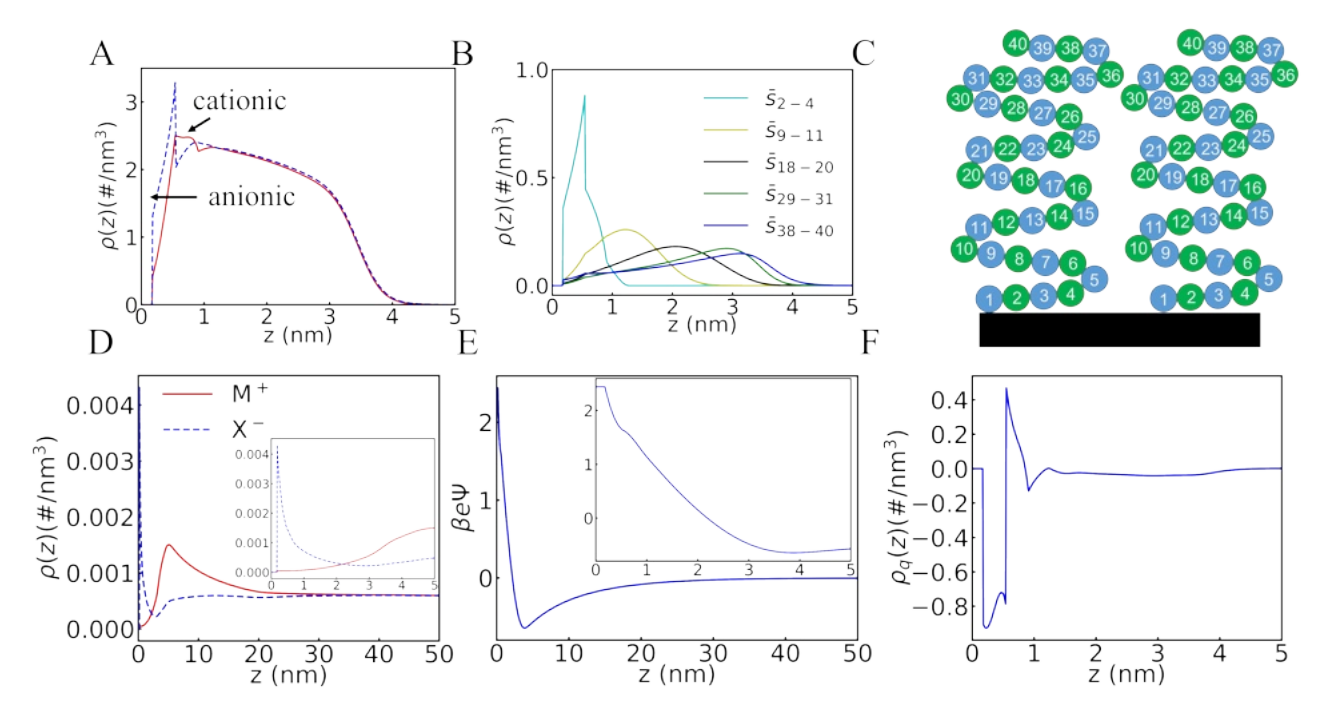


Figure 3: The same as Figure 2 but for an polyampholyte alternating brush  $(AB)_{20}$  with the cationic ends grafted to a neutral surface. (A) Monomer density profiles, (B) segment density profiles averaged over 3 consecutive monomers at different locations along the polyampholyte chain, (C) schematic of the polyampholyte conformation, (D) salt ion density profiles, (E) electrical potential profile, and (F) charge density profile. Here, the grafting density is  $\sigma_g = 0.4 \text{ nm}^{-2}$ , and the salt concentration is  $c_s = 1 \text{ mM}$ . The insets in panels D and E show the corresponding profiles close to grafting the surface, in the range 0-5 nm.

Turning to a polyampholyte brush with an alternating architecture, Figure 3 depicts the microscopic structure at the same salt concentration of  $c_s$ = 1 mM. Broadly speaking, the density profiles for the alternating brush display similar features to those for the diblock case, including the coinciding distributions of cationic and anionic segments (panel A) and EDL formation outside the brush domain (panel E). Upon contrasting the cation and anion

density profiles given in panel D and its inset against those for the diblock case and computing the corresponding excess amounts  $(\Gamma_i = \int [\rho_i(z) - \rho_i^b] dz$ , where 0 < z < 30, it is clear that there is greater accumulation of anions in the brush while the excess cation amount remains similar. Apparently, the local pairing of the oppositely charged monomers makes the structure of an alternating brush look more like that of a neutral brush. As depicted in panel B, there is a correlation between the segment number, sequentially labeled along the polymer backbone starting from the tethered end, and its distance from the grafting surface; specifically, segments located further along the backbone are situated at greater distances from the grafting surface. Schematically, panel C illustrates the structure in an alternating brush, which exhibits an extended conformation similar to that for a neutral brush. In contrast to the back-folding structure observed in the diblock polyampholyte brush described previously, the alternating brush appears slightly more expanded, likely attributable to the wider distribution of polymer segments at the brush surface (panel B). Also noticeable is the fact that the chain is folded considerably in the lateral direction as can be inferred from panel B where all segments are clearly within a distance of 10 segments (4.5 nm) from the surface.

Figure 3E and the inset therein show that, unlike the diblock case where the electric potential is negative virtually throughout the brush, the electrical potential within the alternating brush is positive in a surface region of considerable width ( $\approx 2$  nm). Away from the grafting surface, the electrical potential becomes negative and diminishes smoothly in the remaining region of the brush. The potential profile corroborates the peak density of anions near the surface. The peak position is notably shifted away from the grafting surface because the localized charge of tethered cationic segments is almost completely neutralized by that of their immediate neighboring anionic segments. The distributions of charge species are dictated by strong electrostatic interactions and excluded volume effects, resulting in a strong oscillatory distribution of the local charge at a length comparable to the segment/ion diameter (panel F).

In the brush with an alternating architecture, the positive and negative charges of each polyampholyte chain are located adjacent to each other, which yields greater local charge neutrality than the diblock case. The closeness of polymer charges prevents the build up of ionic species of any particular sign. The region of positive potential for the alternating case, as shown in panel E and reflected in the anion density profile, has a width greater than that for the diblock case due to the stronger constraints of anionic monomers. We speculate that the tethered cationic segments create a region of positive potential away from the grafting surface due to the extended conformation of alternating polyampholyte chains.

#### 3.2. Effects of salt concentration

As mentioned above, previous theoretical studies indicate that the salt concentration plays a major role in determining the swelling behavior of polyampholyte brushes. In particular, the molecular theory of weak diblock polyampholytes<sup>9</sup> predicts that the addition of salt reduces the inter-block attraction and unfolds the polyampholyte chains, leading to an increase of the brush height. Because a strong polyampholyte does not have charge regulation effects in play, it represents an ideal system to decipher the different roles of electrostatic interactions and excluded-volume effects in the swelling behavior.

To investigate the salt effects, we quantify the expansion of polymer chains in terms of the brush height, defined according to the first moment of the segment density profile

$$H_t = \frac{2\int \rho_t(z)zdz}{\int \rho_t(z)dz} \tag{13}$$

where  $\rho_t(z) \equiv \rho_A(z) + \rho_B(z)$  is the total monomer density of polymer segments, with subscripts t, A and B denoting total, cationic and anionic monomers, respectively. For a diblock brush, we can calculate the average heights of individual blocks using the corresponding densities instead of the total monomer density. To quantify the intra-chain complex formation, we define the degree of association in terms of the distributions of cationic (A) and anionic

$$\alpha = 1 - \frac{\int dz |\rho_A(z) - \rho_B(z)|}{2 \int dz \rho_A(z)}$$
(14)

For perfect association by back folding, we have  $\rho_A(z) = \rho_B(z)$  thus  $\alpha = 1$ . Conversely,  $\alpha = 0$  means complete separation or dissociation of cationic and anionic segments in the diblock brushes (since  $\int \rho_A(z)dz = \int \rho_B(z)dz$  for a symmetric diblock brush).

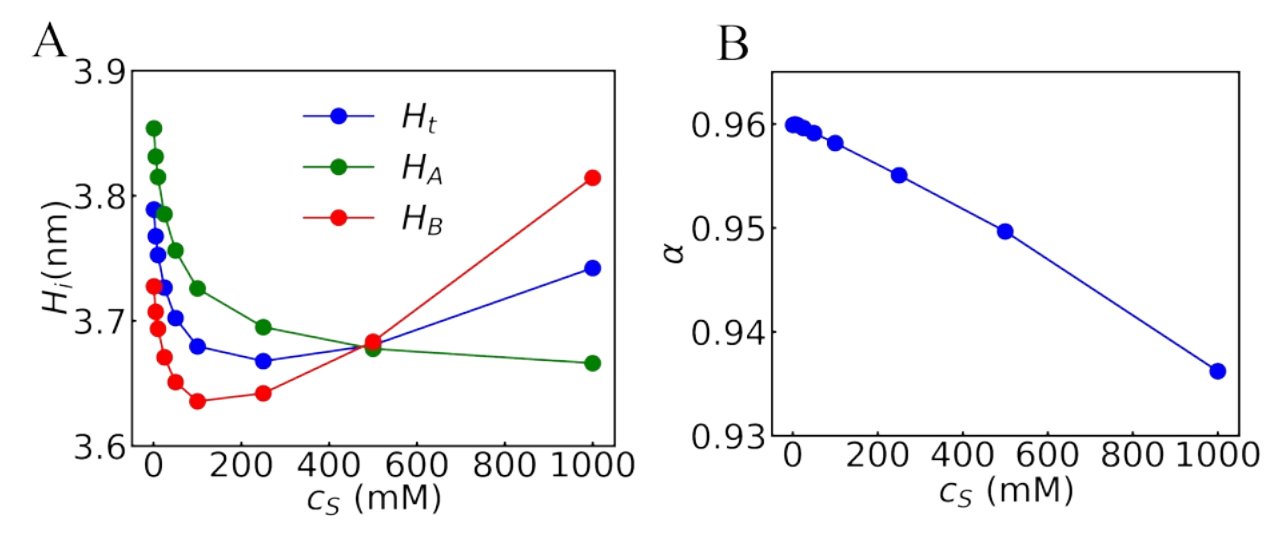


Figure 4: (A) The salt effects on the total brush height  $(H_t)$ , the bottom block height  $(H_A)$ , and the top block height  $(H_B)$ ; (B) The variation of the overlap between two blocks with salt concentration for the diblock brush. Here, the grafting density of polyampholytes is  $\sigma_g = 0.4 \text{ nm}^{-2}$ .

Figure 4A illustrates the changes in the total brush height, along with those of individual blocks, as a function of salt concentration for the diblock polyampholyte brush described earlier. Figure 4B shows the corresponding changes in the degree of intra-chain association. Intuitively, one would expect the brush to extend upon addition of salt due to the screening of electrostatic attraction between positively and negatively charged monomers. While the increased ion screening reduces the degree of association between the cationic and anionic blocks, the brush height initially falls upon the addition of salt before increasing at higher salt concentration, in contrast to the monotonic trend predicted by the molecular theory for weak polyampholyte brushes. The initial regime of height decrease extends over a wide range of salt concentration (up to 250 mM). Moreover, the lower (cationic) block undergoes

shrinkage upon the addition of salt across the entire studied concentration range, albeit with a diminishing rate of decrease at higher salt concentrations. Conversely, the brush height associated with the upper (anionic) block decreases for salt concentrations up to approximately 100 mM, after which it experiences a rapid increase at higher salt concentrations. At 1 M salt concentration, the total brush height is less than that in the limit of zero salt concentration because, as indicated by the green curve, the lower block decreases its height monotonically as the salt concentration increases. Meanwhile, the interblock attraction is significantly reduced at high salt concentration, which leads to the outer block being more extended. It can be expected that a further increase in the salt concentration will ultimately lead to the total height of the brush exceeding that of the zero salt case. In addition, as anion size decreases, the brush height becomes more sensitive to the salt concentration as seen later in Figure 8.

To understand further the non-monotonic trends of the diblock swelling, we plot in Figures 5 and 6 the density profiles of polymer segments and salt ions with increasing salt concentration. Figure 5A shows that, when the salt concentration increases from 1 mM to 250 mM, the density profiles of both cationic and anionic monomers shift toward the grafting surface, leading to the shrinkage of the polyampholyte brush. This trend is also reflected in the density profiles of individual segments as shown in Figure 5 C. Likewise, panel B indicates that as salt concentration rises, the disparity between the bulk salt concentration and the salt concentration within the brush diminishes, suggesting a trend towards greater neutralization of the brush at higher salt concentrations. Nevertheless, an enrichment of anions in the brush is observed at all salt concentrations. The increase in free ion concentration in the brush explains the reduction of intra-chain association with the addition of salt. While the disassociation between the cationic and anionic blocks reduces the stiffness of the polymer backbone, the compression of both blocks with salt addition can be attributed to the reduction of intra-block repulsion, which may not be captured by mean-field theories due to the neglect of connectivity-induced correlations. This is evident from the results obtained on

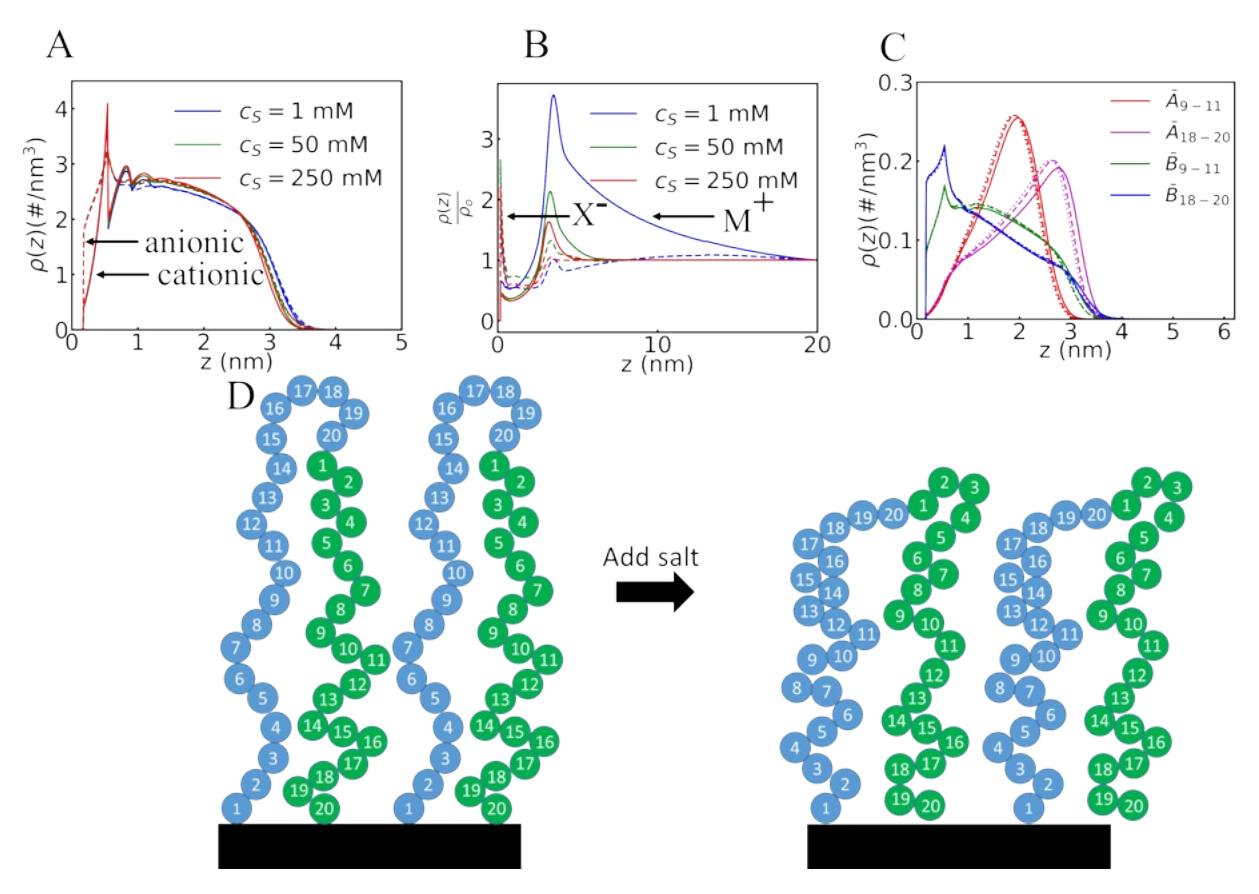


Figure 5: The structure of a diblock polyampholyte brush at different salt concentrations. (A) Monomer density profiles; (B) salt ion density profiles normalized to the bulk salt concentration; (C) segment density profiles at  $c_s = 1$  mM (solid lines) and 250 mM (dashed lines); (D) the change in the polymer conformation as the salt concentration increases.

switching off size-related correlations (hardcore and electrostatic), which show a monotonic increase in total height as well as the individual block heights (Figure S8 in supplementary information material). We also notice in the same plot that the absolute values of heights are much smaller and the degree of overlap is larger when correlation effects are ignored, suggesting stronger contribution of electrostatic attraction to brush thermodynamics. It is noteworthy that deactivating electrostatic correlations and only activating hardcore effects leads to almost the same height values (Figure S9 in supplementary information material) as in Figure 4, which proves short-range electrostatic correlations to be the sole factor behind the observed non-monotonous trend in height vs salt concentration. The collapse of the polymer blocks and disassociation are reflected in the density profiles of individual segments

as shown in Figure 5C. Schematically, panel D depicts the resulting conformational changes. Interestingly, both cations and anions are enriched at the brush surface, reflecting a strong accumulation of anions near the grafting surface and that of cations at the brush edge due to the presence of anionic monomers in that region. Because the tethering of cationic block attracts extra anions, the net charge inside the polyampholyte brush remains negative but its magnitude decreases with the salt concentration.

Figure 6 shows the density profiles of monomers and salt ions at higher salt concentrations. Panel A shows that the density profile for the cationic block (in panel A) does not vary appreciably with the salt concentration in the range of 250-1000 mM, suggesting the limited effects of free anions due to their similarity to the anionic monomers. However, the anionic block extends further away from the surface as the salt concentration increases. The trend is also reflected in the segment density profiles shown in panel C. At low salt concentrations, the brush height can be rationalized in terms of the stiffness of the polymer backbone. Conversely, at high salt concentrations, the expansion of the B block occurs due to the reduction of inter-block attraction. Schematically, panel D shows the conformational changes corresponding to the expansion of the B block. Panel B presents the relative ionic densities at different salt concentrations. The reduction in the relative cation density at the brush surface suggests that the polyampholyte brush is further neutralized at higher salt concentrations.

Now turning to the alternating brush, Figure 7 shows the variation of the total brush height with salt concentration along with the density profiles of different polymer segments. In the low salt concentration regime ( $c_s$ = 1, 5, 10 mM), we observe a slight reduction of the brush height with increasing salt concentration. While the addition of salt has multiple effects, the reduction in brush height is probably because of the screening of both inter-chain and intra-chain repulsion by salt ions. While the alternating brush is almost everywhere neutral, the alternating architecture generates an effective dipole along the polymer backbone and their alignment may lead to strong intra-chain repulsion. As shown in Panel B, the

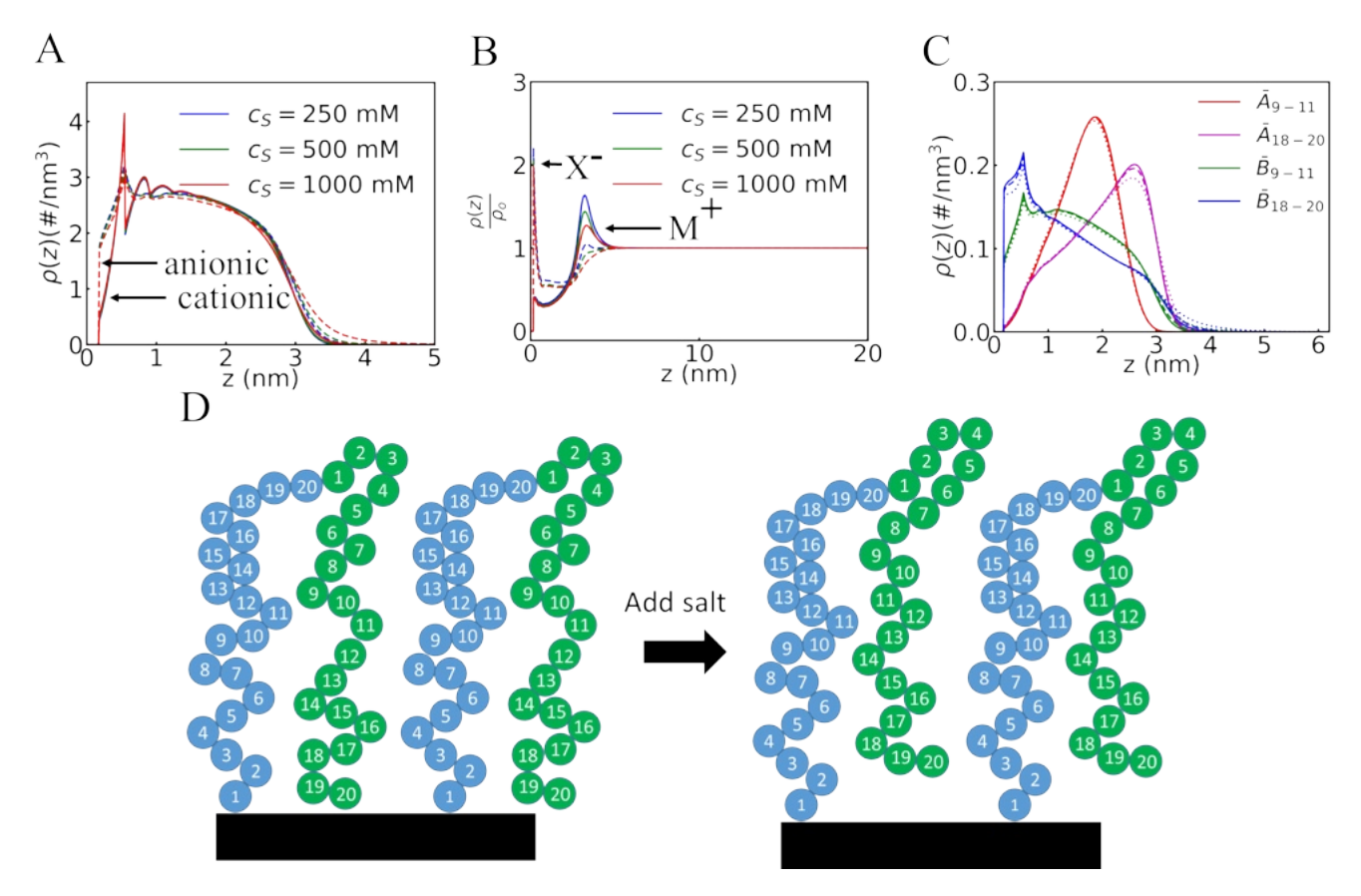


Figure 6: The same as Figure 5 but at higher salt concentrations ( $c_s = 10, 250, 1000 \text{ mM}$ ).

segment densities are relatively insensitive to the increase in the salt concentration, and the change in the brush structure occurs mostly at the outermost polymer segments ( $\bar{s}_{38-40}$ ). In contrast, the alternating brush expands in the high salt concentration regime probably due to the reduction of the intra-chain attraction. It could also be likely that the condensation of salt ions onto their respective oppositely charged monomers, leading to overcharging and expansion of the brush at high salt concentrations.

#### 3.3. Effect of anion size

As noted in the introduction, the size of free ions can play a crucial role in governing the structural properties of charged polymer brushes. To examine its effects in two-component charged brushes, we may vary the anion size while keeping the sizes of other species un-

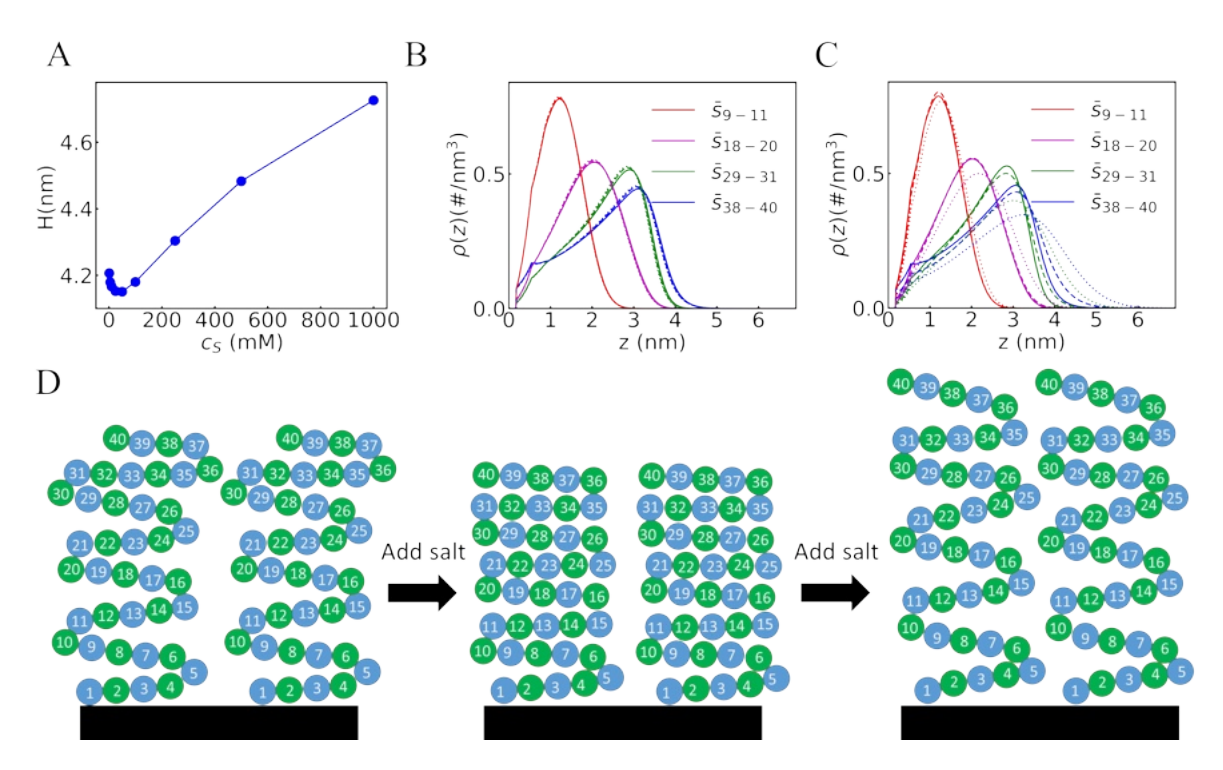


Figure 7: Salt effects on an alternating polyampholyte brush. (A) The variation of brush height with salt concentration; (B) the segment density profiles in the low salt concentration regime ( $c_s$ = 1, 5, 10 mM); (C) the segment density profiles in the high salt concentration regime ( $c_s$ = 10, 250, 1000 mM); (D) schematic of the conformational changes upon salt addition. In panels B and C, the solid lines represent the lowest salt concentration, the dashed lines the intermediate salt concentration, and the dotted lines the highest salt concentration.

changed. Figure 8 shows the dependence of brush height on the anion size at different salt concentrations for the alternating brush discussed above. At low salt concentrations, the brush height exhibits only a marginal dependence on the anion size, with larger anions resulting in slightly increased brush heights. At high salt concentrations (here beyond about 250 mM), the brush height demonstrates an inverse dependence trend on the ion size. The relative electrostatic interaction between the positively charged monomer and anions across different sizes can be roughly approximated in terms of the Coulombic potential at contact. In essence, the smaller the anion, the more pronounced its interaction with the positively charged monomers, resulting in a greater extent of neutralization of the positively charged monomers. In other words, the strong association between anions and cationic monomers makes the alternating brush behave like one with negatively charged polyelectrolytes, which

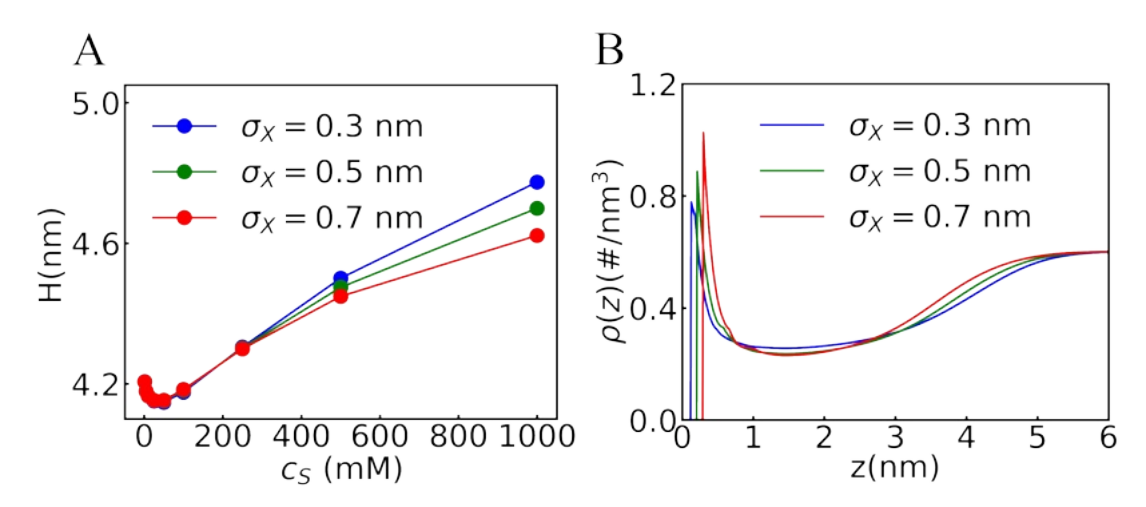
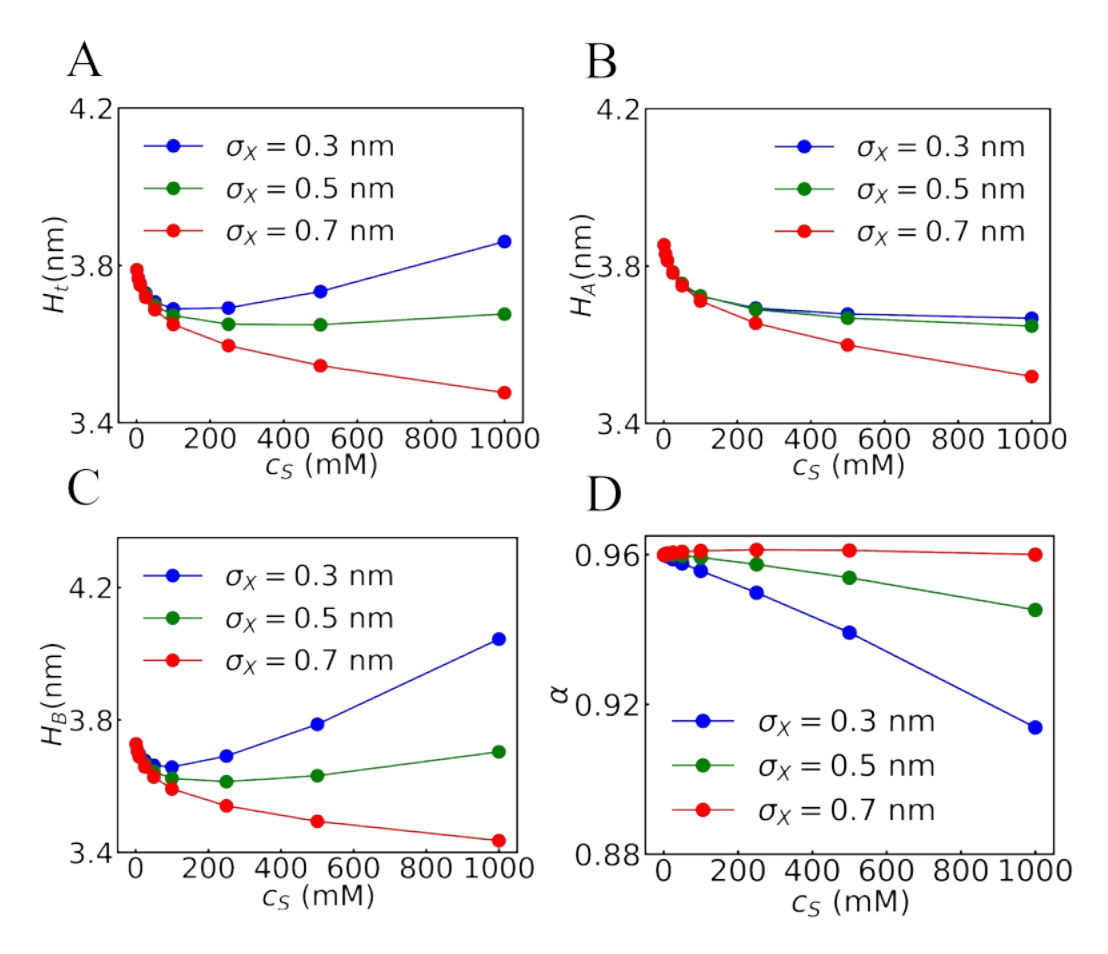


Figure 8: (A)The variation of the brush height for an alternating brush with salt concentration at different anion sizes. The grafting density and the chain length are the same as those for the diblock system. (B) anion density profile as a function of anion size at  $c_s$ =1000 mM.

is also supported by the sign reversal of the electric potential profile with decreasing anion size at  $c_S = 1000$  mM, as shown in Figure S3 of SI. The brush extends due to the increased repulsion between negatively charged monomers. Additionally, a complementary mechanism contributing to this trend could stem purely from excluded volume effects. Panel B in Figure 8 shows the anion density profiles at  $c_s = 1000$  mM. The anions are distributed further from the inner region of the brush as their size increases, which can be attributed to the increased work required to confine ions within this region due to excluded volume effects. Interestingly, a reverse trend is observed in the outer region because the larger anions, in turn, reduces the screening of attractive interactions, making the brush less extended. The above behavior in the high salt concentration regime has similarity to ellipsometry data on anion size dependence of zwitterionic poly(cysteine methacrylate) (PCysMA) brush height.<sup>8</sup> Experimentally, the brush height was seen to increase with higher salt concentration and to vary with the anion size in the order of SCN<sup>-</sup> > NO<sub>3</sub><sup>-</sup> > Br<sup>-</sup> > Cl<sup>-</sup>  $\approx$  SO<sub>4</sub><sup>2-</sup>. Because SCN<sup>-</sup> is only weakly hydrated, it has a small effective ion size and interacts most strongly with the polymer. Conversely,  $SO_4^{2-}$  is strongly hydrated in water, making its effect on the brush height less pronounced than SCN<sup>-</sup>. It is crucial to emphasize that the concordance



**Figure 9:** The variation of (A) the brush height  $(H_t)$  (B) the bottom block height  $(H_A)$  (C) the top block height  $(H_B)$  (D) the degree of overlap between two polyampholyte blocks with salt concentration at different anion sizes.

between our findings and experimental observations should be interpreted solely in terms of the general trend rather than as a precise quantitative match. This is primarily because the zwitterionic system contains charges in its side chains, and furthermore, the monomers are ionizable. The variation of electrostatic interaction strength with the size of anions can also alter the dissociation equilibrium, further complicating direct comparisons.

Turning to the diblock case, panel A in Figure 9 illustrates the dependence of the brush height of the diblock brush on the anion size in the same concentration range as the alternating brush. At low salt concentrations, the curves for different anion sizes overlap similarly to the alternating case, indicating that the system is relatively insensitive to changes in anion size. At higher salt concentrations, the re-entrant behavior, which is seen for the

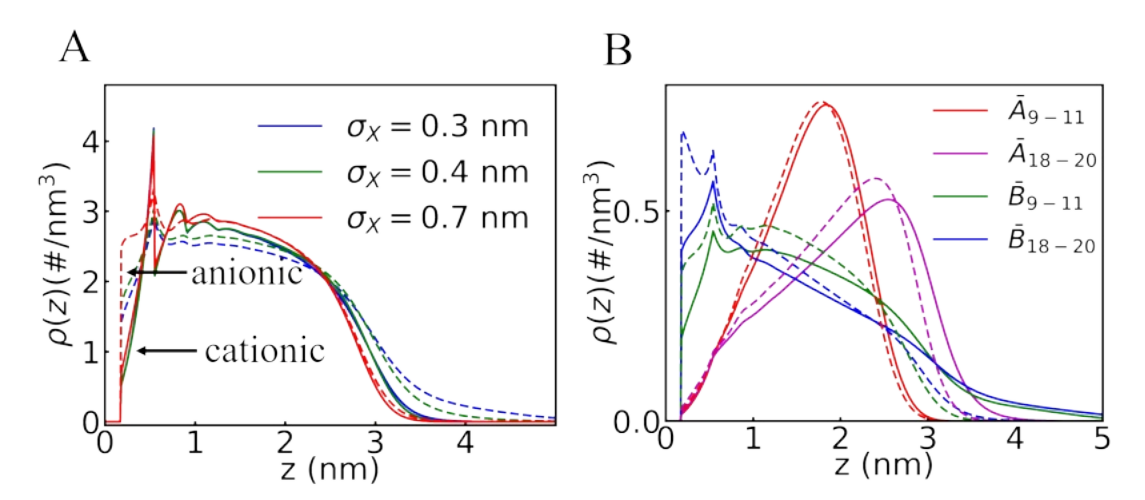


Figure 10: (A) The variation of monomer density profiles with anion size in the diblock system. The solid lines represent A monomer density profiles while the dashed lines represent B monomer density profiles. The salt concentration is 1000 mM. (B) The segment density profiles at the same condition. The solid lines correspond to  $\sigma_X = 0.3$  nm and the dashed lines correspond to  $\sigma_X = 0.7$  nm.

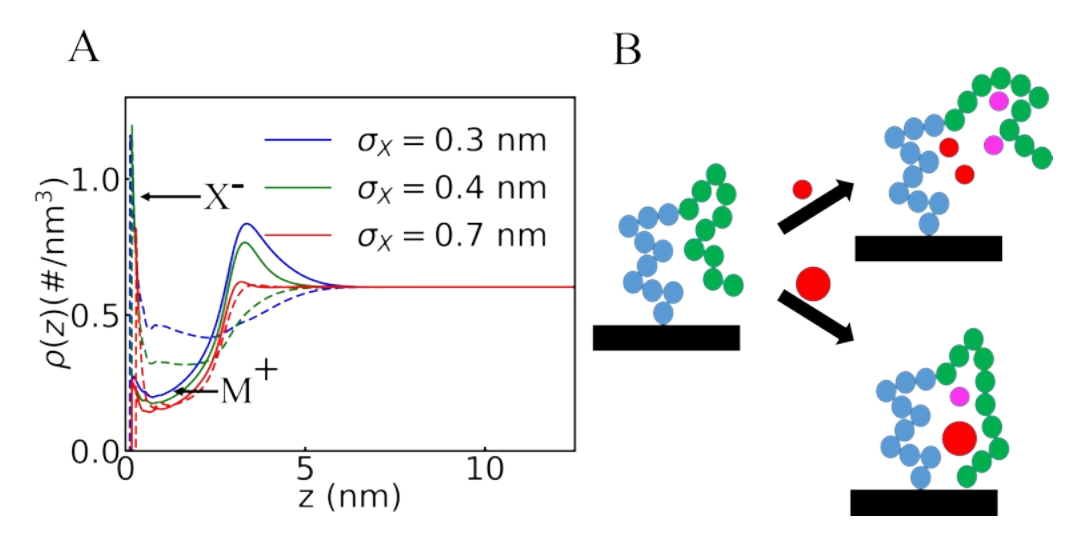
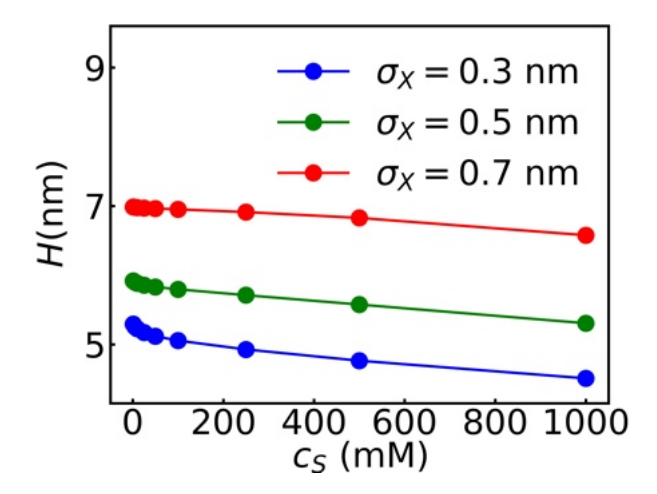


Figure 11: (A) The variation of cation and anion density profiles with anion size at 1000 mM salt concentration. The solid lines represent anion density profiles while the dashed lines represent cation density profiles. (B) The conformational states of the polymer chain under small anion and large anion conditions. The pink spheres represent the cation and the red spheres represent the anion.

alternating case across all anion sizes, disappears as the anion size is increased, leading to a monotonic decline of the brush height as salt concentration increases. Nevertheless, for small sized anions, the re-entrant behavior persists with a small height increase at high salt

concentrations. A comparison of Figures 8A and 9A indicates that the total height increase for the block case across the considered range of salt concentrations for small anion sizes ( $\sim 0.2$  nm for  $\sigma_X = 0.3$  nm) is considerably smaller than the corresponding values for the alternating case ( $\sim 0.65$  nm for  $\sigma_X = 0.3$  nm). Furthermore, an analysis of the lower block height plots, shown in Figure 9B, and the upper block thickness plot, shown in Figure 9C, reveals that large sized anions compress both the lower block and the upper block more than their small sized counterparts. Similarly,  $\alpha$  vs  $c_S$  plots, presented in panel D of the same figure, show that for small anion sizes, the self-association of polyampholytes decreases with increasing salt concentration, whereas for large anion sizes, the self-association remains virtually unchanged with variations in salt concentration. To understand the underlying structural changes in the brush, we plot the monomer density profiles as well as the end segment density profiles in Figure 10 for different anion sizes at a salt concentration of 1000 mM. It is seen that as the anion size decreases, both A and B monomer density profiles stretch away from the surface with the extent being higher for the outer (B) block. Also, the segment density profiles  $(\bar{A}_{18-20}, \bar{A}_{15-17}, \bar{B}_{9-11} \text{ and } \bar{B}_{18-20})$  for the lowest sized anion are also most stretched out, indicating the unfolding of the brush. To understand the driving force behind this behavior, we present in Figure 11 the corresponding cation and anion density profiles. It is seen that reducing the anion size increases the concentration of both anion and cation inside the brush. This can be attributed to decreased excluded volume interactions between anions and the brush for small sized anions as well as higher electrostatic attraction at contact between monomers and small sized anions. Consequently, there is enhanced screening of electrostatic attraction between the lower block and the upper block and the resulting reduced electrostatic attraction separates the two blocks apart, causing an increase in brush height for small anions.

The above-mentioned size-dependence of salt response displayed by both diblock and alternating polyampholytes is in contrast with that in single component cationic polyelectrolyte brush systems. Figure 12 depicts the size dependence of height vs salt concentration



**Figure 12:** The variation of the brush height for a single component cationic brush with salt concentration at different anion sizes. The grafting density and the chain length are the same as those for the studied polyampholyte system.

curves for a single component polyelectrolyte brush of the same chain length and grafting density. In all cases, the brush does not exhibit a transition from the osmotic regime to the salted regime. We may estimate the crossover concentration from the salt concentration at which the ion concentration inside the brush is equal to that in the bulk. The ion concentration inside the brush can be approximated by

$$c^* = \frac{\rho_g A N_P}{A L} \approx \frac{\rho_g A N_P}{A N_P \sigma_P} = \frac{\rho_g}{\sigma_P},\tag{15}$$

where A is the surface area, and L is the brush thickness. In the above equation, we assume that the polymer chains have a fully extended conformation, i.e., L is equal to the chain length  $N_P$  multiplied by the segment diameter  $\sigma_P$ . The assumption is reasonable for a polyelectrolyte brush in the osmotic regime. The estimated crossover concentration is 1.5625 M, above the salt concentration range used in our work. Increasing the anion size results in the brush swelling, while increasing salt concentration reduces the brush height for all anion sizes. As illustrated in Figure S4B, the elevated ion concentration within the brush for small counterion sizes results in lower electrostatic repulsion among monomers. This is reflected in the decrease in electric potential throughout the brush as shown in panel C of

the same figure. Additionally, a smaller anion size also decreases excluded volume repulsion, as evidenced by the diminishing oscillations of the corresponding monomer density profiles (panel A in the same figure). The reduced electrostatic repulsion among polymer segments explains the monotonic reduction of the brush height with increasing salt concentration.

#### 3.4. Effect of cation size

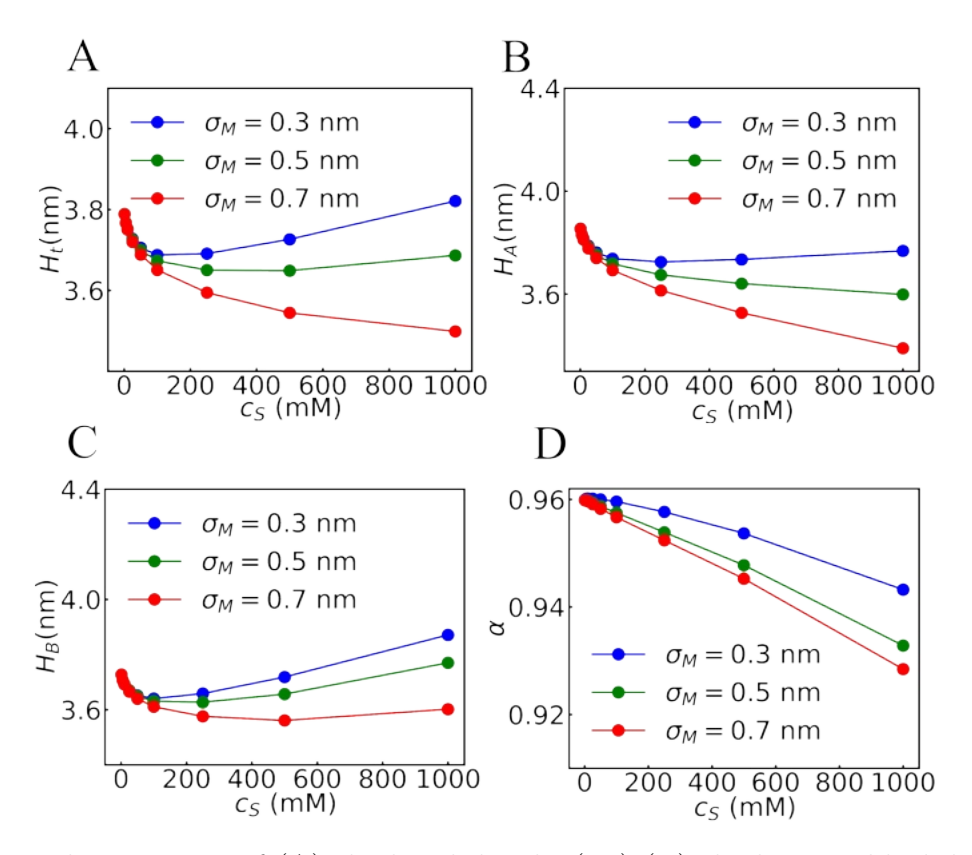


**Figure 13:** The variation of (A) the brush height  $(H_t)$  (B) the bottom block height  $(H_A)$  (C) the top block height  $(H_B)$  (D) the degree of overlap between two blocks with salt concentration at different cation sizes.

In this section, we investigate the response of the brush swelling to the variation of the size of the counterions to the upper block of a polyampholyte brush. Here, we confine our investigation to the diblock architecture because the alternating brush is anticipated to elicit a similar response to variations in both anion and cation sizes, owing to the proximity of charges along the chain. Figure 13 shows the dependence of the total brush height, A block

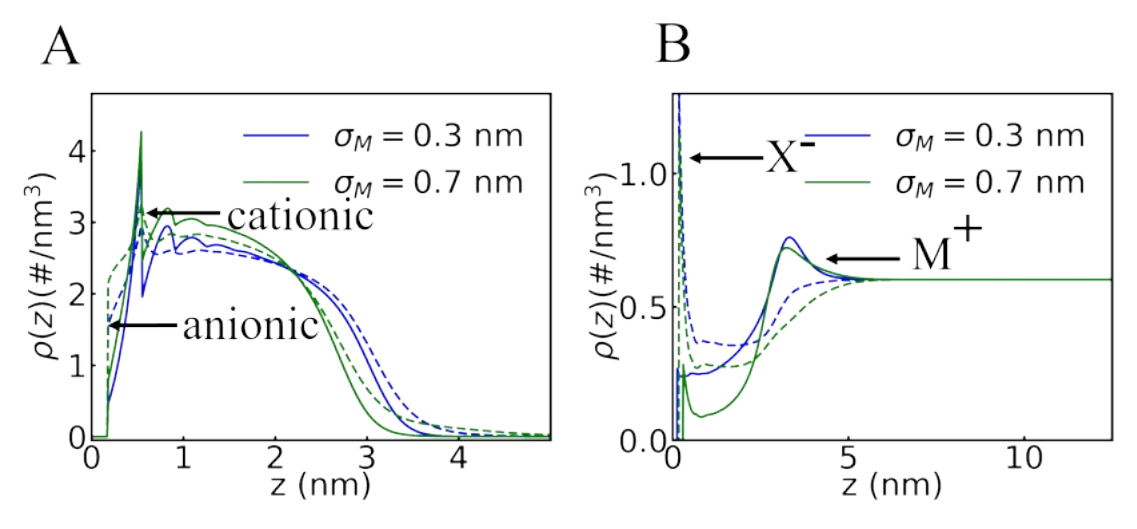


**Figure 14:** (A) The variation of A (solid lines) and B monomer (dashed lines) density profiles with cation size at 1000 mM salt concentration. (B) The variation of cation (dashed lines) and anion (solid lines) density profiles with anion size under same conditions.

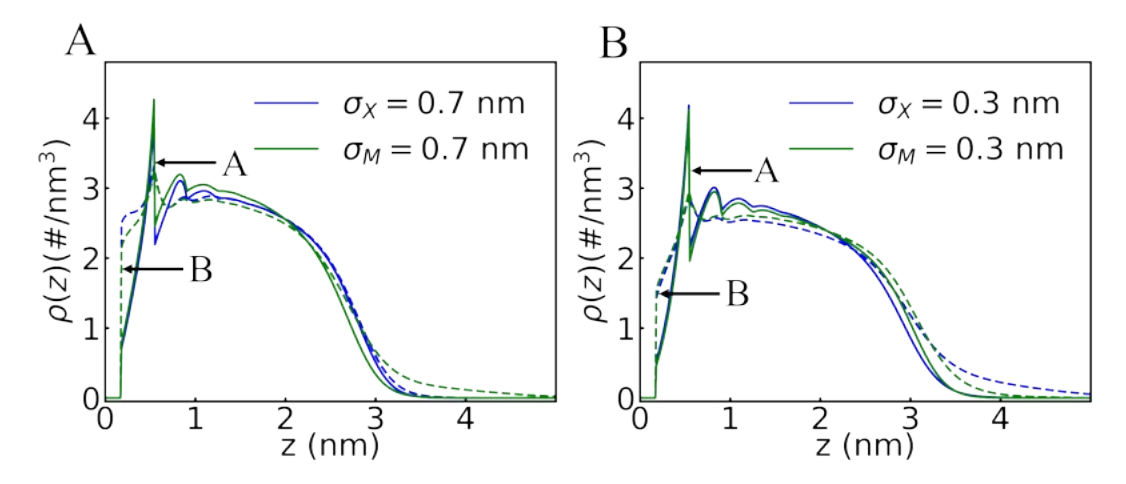
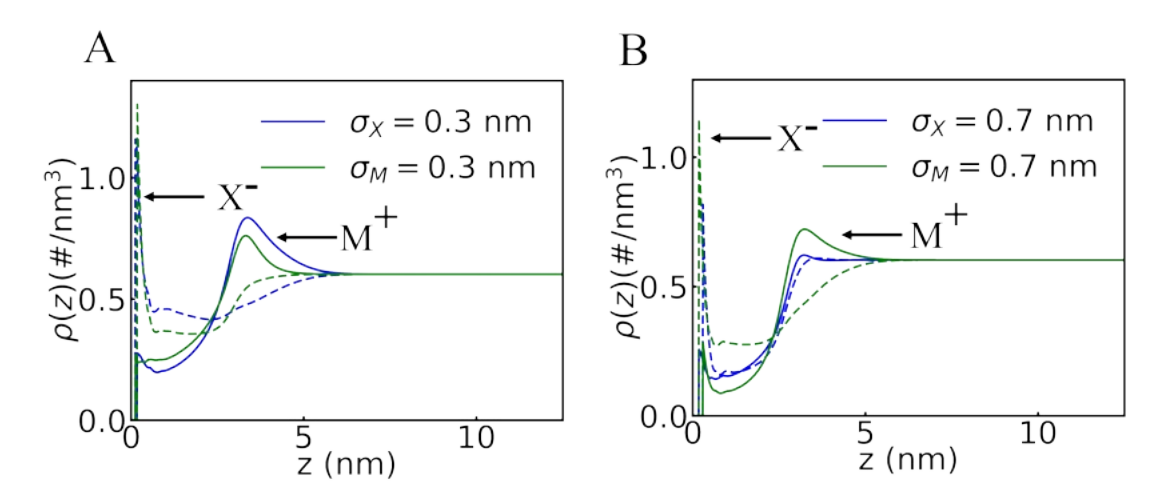


Figure 15: panel (A) - A (solid lines) and B monomer (dashed lines) density profiles in two cases; (1) the anion is bigger than the rest of the species  $\sigma_X$ =0.7 nm (2) the cation is bigger than the rest of the species  $\sigma_M$ =0.7 nm. The salt concentration is 1000 mM. panel (B) - A (solid lines) and B monomer (dashed lines) density profiles in two cases; (1) the anion is smaller than the rest of the species  $\sigma_X$ =0.3 nm (2) the cation is smaller than the rest of the species  $\sigma_M$ =0.3 nm.

height, B block height, and the overlap parameter on the salt concentration for three different cation sizes. It is seen that the qualitative trends for the first three quantities with respect to salt concentration stay approximately the same here as in the case where the anion size was varied. Quantitatively, the decrease in  $H_A$  with increasing  $c_s$  is slightly more for larger sized



**Figure 16:** Counterion and coion density profiles under the same conditions as Figure 15

ions and there is saturation or a slight increase in  $H_A$  at high salt concentrations for  $\sigma_M = 0.3$ nm. Similarly, for a given salt concentration, the variation in  $H_B$  with  $\sigma_M$  is less pronounced than the variation in  $H_B$  with  $\sigma_X$ . However, the most distinctive aspect here, in terms of differentiation from the case of anion size variation, is that  $\alpha$  decreases with increasing  $\sigma_M$ . This means the overlap between polyampholyte two blocks decreases with increasing cation size, a trend opposite to what was seen when anion size was varied. A close examination of A and B monomer density profiles at two extreme sizes ( $\sigma_M = 0.3$  nm and 0.7 nm) (panel A in Figure 14) reveals that both blocks move towards the surface with increasing cation size, and the gap between their profiles slightly grows. This observation is counter-intuitive because a larger cation excludes both cations and anions from the brush (panel B in Figure 14), which should decrease the overlap between two blocks due to enhanced electrostatic interactions. Because the cations have to locate in the outer region due to a higher amount of charge imbalance between monomers, there is insignificant variation in their concentration with their size and hence, the difference in electrostatic screening exerted by ions is small. However, this closeness of concentration values implies that for large sized ions, there is a higher amount of excluded volume pressure, which prevents the two blocks from overlapping. This is also reflected in the electric potential profile (Fig. S5) for  $\sigma_M=0.7$  nm, which has both positive and negative regions, each corresponding to the location of the monomers of the same polarity. In contrast, the local electric potential is always positive for  $\sigma_M = 0.3$ nm. Note that these variations in the overlap with cation size are very small compared to the values seen for the case when anion size is varied. Another noticeable observation is when the size of the varying ionic species is large, the overlap is greater in the case of anions than in the case of cations. This is clearly evident in the monomer density plots for A and B at  $\sigma_M$ =0.7 nm and  $\sigma_X$ =0.7 nm. On the other hand, a reverse trend is observed for  $\sigma_M$ =0.3 nm and  $\sigma_X$ =0.3 nm. The corresponding density profiles of polymer segments and free ions are shown in Figures 15 and 16. A comparison of the counterion density profiles in Figure 11A and Figure 14B indicates that there is more depletion of both ions near their respective oppositely charged monomers in the brush for  $\sigma_X=0.7$  nm than for  $\sigma_M=0.7$  nm (also shown in Figure 16B). In the former case, the larger ion must penetrate deeper into the brush to approach its corresponding oppositely charged monomer. Conversely, in the latter case, the ions only need to remain in the distal part of the brush. In the latter case, it is the more effective cancellation of monomer charge due to the enhanced ion concentration that keeps the two blocks apart, resulting in a lower degree of block overlap. In terms of  $\sigma_M$ =0.3 nm and  $\sigma_X=0.3$  nm, the counterions to the bottom part of the brush (X) have a larger radius  $(\sigma_X = 0.4 \text{ nm})$ , leading to more ion depletion and thus a higher degree of overlap in the brush for  $\sigma_M = 0.3$  nm than for  $\sigma_X = 0.3$  nm as shown in panel A of Figure 16.

## 3.5. Valency effects on polyampholyte brushes

Lastly, we examine the impact of cation valency on the structural behavior of both alternating and diblock sequences. Figure 17 presents the salt effects on the brush height as well as individual block heights alongside the degree of overlap between oppositely charged blocks for the diblock case but with divalent cations. Similarly, Figure 18 presents the height variation of the alternating brush.

Several features become evident upon comparing the swelling behaviors under divalent salt conditions with monovalent salt conditions, as well as between the two polyampholyte

architectures. Firstly, the brush height is larger for both architectures under divalent ion conditions compared to monovalent ion conditions. In the diblock case, the alteration of the lower block height with salt concentration mirrors that observed in the monovalent salt case. The majority of structural changes occur within the upper block. A stronger binding of free ions to the polymer is also reflected in the lower  $\alpha$  values for the divalent case. The larger brush height for divalent cations can also be attributed to enhanced screening effects for attraction between opposite charged polyampholyte blocks. Secondly, the height increase upon salt addition is higher for the alternating brush and the reentrant behavior is almost diminished compared to the diblock case. This again can be understood in terms of the localization of the cations in the diblock case (Fig. S6). The self-repulsion between negatively charged monomers is restricted to the lower part of the brush, and the brush extension would be limited due to chain elasticity. On the other hand, for the alternating brush case, the negatively charged monomers are distributed across the whole chain contour (Fig. S7). This leads to the extension of the whole brush and hence, an increased brush height. In the experimental literature, ion specificity under divalent cationic salt conditions was observed for zwitterionic PCysMA brushes.<sup>8</sup> In that case, Ba<sup>2+</sup> was seen to swell the brush more than  $Ca^{2+}$ .  $Ba^{2+}$  is slightly less hydrated than  $Ca^{2+}$ , possessing a smaller effective radius. The trend agrees with the existence of an inverse relation between brush height and the free ion size obsvered in this work. In the same experimental study, it was also observed that monovalent anions would swell the brush more than divalent cations, which is in contrast with our results. A possible reason could be the hydrated anions are considerably smaller than hydrated cations and hence, anions interact more strongly with monomers than cations, resulting in a greater reduction of attraction between oppositely charged monomers. In our study, no distinction was made between anions and cations in terms of their hydration ability since the studied size range is the same for both of them. In the above-mentioned experimental study,  $Y^{3+}$  was seen to collapse the brush at intermediate concentrations. We did not notice any such trend in our theoretical results (not shown here). Attenuated total reflection Fourier transform infrared spectroscopy (ATR-FTIR) study on the same system revealed the presence of monodentate, bridging bidentate, and chelating bidentate coordinations of carboxylate groups with divalent and trivalent cations. Apart from the difference in architecture, these specific mechanisms of ion coordination might be a potential source of the disagreement noted above.

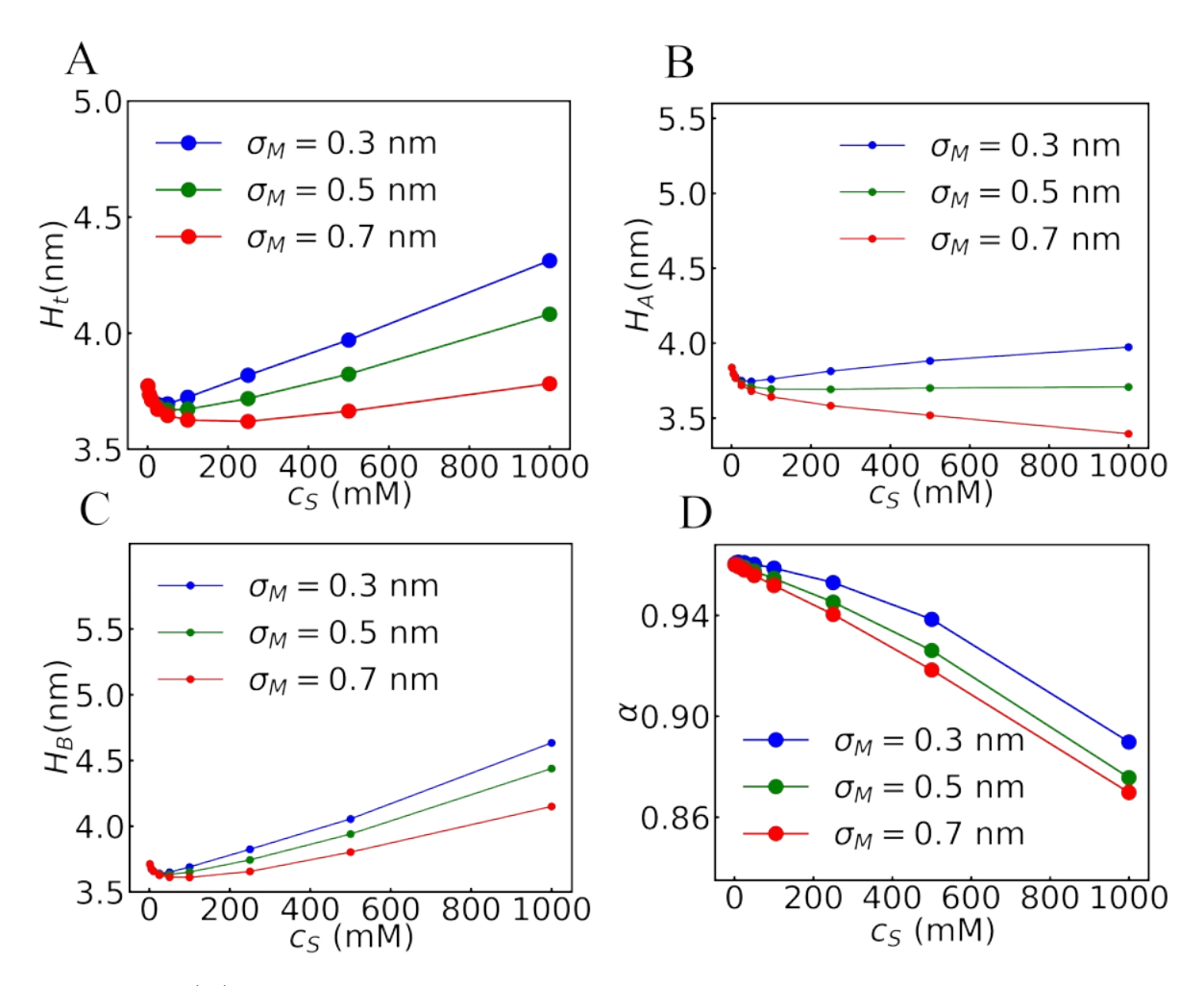


**Figure 17:** (A)The variation of the brush height for a diblock brush with divalent salt concentration at different cation sizes. The grafting density and the chain length are the same as those given previously for monovalent systems. (B) The corresponding plots for overlap parameter variation.

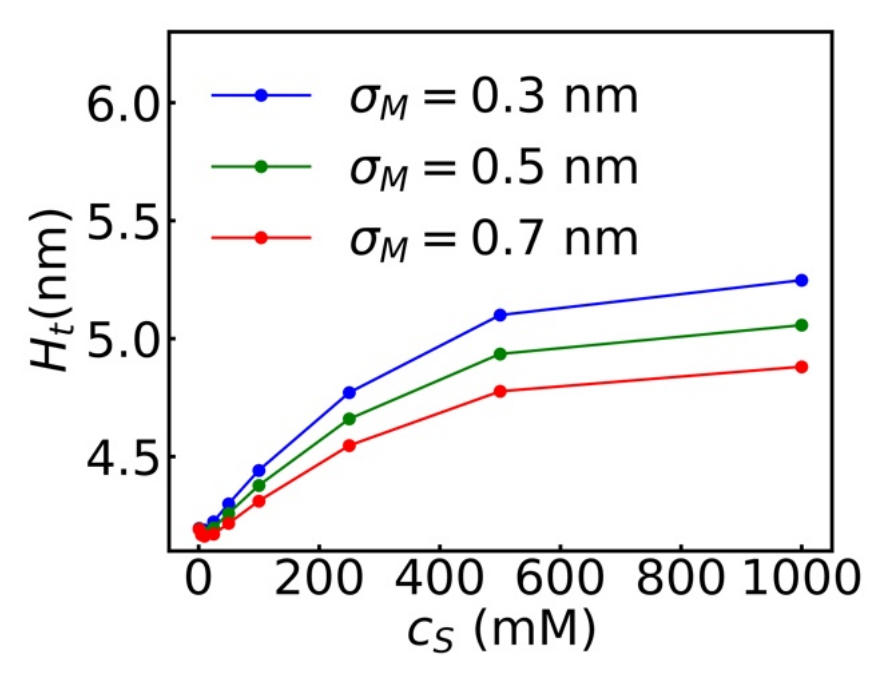


**Figure 18:** The variation of the brush height for an alternating brush with divalent salt concentration at different cation sizes. The grafting density and the chain length are the same as those given previously for monovalent systems.

#### 4. Conclusions

In this study, we employed classical density functional theory (cDFT) to conduct a thorough investigation into the response of strong polyampholyte brushes to ion size and valence over a range of salt concentrations. Specifically, we characterized the structural behavior of polyampholyte brushes with diblock and alternating architecture brushes by examining their height and ion distributions. For diblock brushes, an analysis of the height of each individual block, as well as the monomer density profiles of both blocks and the density profiles of segments, revealed that in the absence of salt, the polyampholyte adopts a fully collapsed conformation. In this state, the top block bends back into the lower block, forming positively and negatively charged monomer pairs. In contrast, due to the proximity of oppositely charged monomers along the chain, the alternating brush behaves like a neutral brush with a height exceeding that for the diblock brush. If all monomeric species and free ions have the same size, the increase in salt concentration would first reduce the brush

height, followed by brush swelling at higher salt concentrations. The non-monotonic trend suggests a reentrant behavior in response to the salt concentration. In the diblock case, an analysis of the individual block heights and the monomer density profiles showed that the lower brush height always decreases while the upper block height follows the same trend as the overall brush height. This non-monotonic behavior of the brush height in both architectures stands in contrast to the anti-polyelectrolyte effect, which predicts an increase in brush height with the addition of salt due to the weakening of electrostatic attraction between two blocks. We attribute this difference primarily to the interplay between two competing factors, namely electrostatic repulsion between monomers of the same block and electrostatic attraction between monomers of dissimilar blocks. The effects of excluded volume interactions become evident when the size asymmetry is introduced between free ions and monomeric species. For diblock brushes, when the size of the counterions to the lower block is increased, the abovementioned reentrant behavior gradually disappears, yielding a monotonic decrease in the total brush height with the increase in the salt concentration. On the other hand, when this counterion is made smaller than the monomer size, the reentrant behavior becomes magnified. An analysis of cation and anion density profiles revealed that the densities of both ions inside the brush is highest for the smallest anion and lowest for the largest anion. For small anions, the enhanced ion concentration within the brush reduces the electrostatic attraction between oppositely charged monomers, leading to the unfolding of the self-associated polyampholyte chains. Conversely, the decreased concentration of ions for large sized anions enhances the attraction between two blocks of polyampholyte chains, causing a reduced brush height. For the alternating brush, however, the reentrant behavior is observed across all anion sizes, and at high salt concentrations, smaller ion sizes result in greater brush heights. When varying the size of cations, which serves as the counterion to the top block, the trends regarding the brush height are similar to those corresponding to alternating brushes. However, the degree of overlap between the two polyampholyte blocks decreases with increasing cation size, which contrasts with the trend observed in the case of anions. The theoretical results can be rationalized in terms of the higher excluded volume pressure in the case of bigger cations, which are localized in the outer part of the brush, and the resulting resistance to outer block folding. Finally, we studied the brush structural properties for divalent salts and found that the brush height is higher than for monovalent salts for both architectures, which could be attributed to stronger screening of oppositely charged monomer interaction. Moreover, the reentrant behavior vanishes for alternating brushes, and instead, a more substantial increase in height is observed.

To our knowledge, this work represents the first comprehensive study of polyampholyte brushes in response to variations in ion size, valency, and salt concentration. We offer novel insights into polyampholyte brush systems such as the reentrant behavior the brush swelling and its dependence on the brush architecture. A few possible extensions of this work would further improve our understanding of the specific ion effects in polyampholyte systems. First, the polyelectrolyte brushes may consist of ionizable segments. In the experimental literature, most brushes studied have weak electrolyte moieties on them and hence, it would be crucial to incorporate charge regulation effects. The recently developed single-chain-inmean-field density functional theory in our group would be ideal for this purpose since it includes electrostatic correlations between monomer groups beyond nearest neighbor pairs. 42 Secondly, it would be interesting to incorporate the coordination ability of multivalent ions into the theory to obtain the underlying physical mechanisms behind the diminishing of anti-polyelectrolyte effects in their presence. 8 Thirdly, an attempt can be made to facilitate a direct comparison between experimental results and cDFT predictions by solving the theory for polymer chains with side groups. In the experiments, 43 increasing the spacing along the side chain between cationic and anionic monomers was seen to be influencing the hydration of monomers significantly. The study proposed above would help incorporate these control parameters. Lastly, it would be interesting to consider the lateral correlation effects in the study. Recently, MD simulations on polyelectrolyte brushes revealed that increasing the multivalent counterion size changed the morphology of the brush from laterally homogeneous collapsed brush to heterogeneous pinned-micelle to vertical phase separated double-layered structure to vertically stretched brush progressively. 44 It would be interesting to see how this lateral correlation affects the charging of the brush and hence the resultant brush height.

## Acknowledgement

This research is made possible through financial support from the NSF-DFG Lead Agency Activity in Chemistry and Transport in Confined Spaces under Grant No. NSF 2234013. Furthermore, AG thanks the support by the National Science Foundation under Grant # EEC-2127509 to the American Society for Engineering Education.

# **Supporting Information**

The Supporting Information presents the detailed equations for the excess free energy and additional numerical results for the microscopic structure of polyampholyte brushes.

## References

- (1) Dobrynin, A. V.; Colby, R. H.; Rubinstein, M. Polyampholytes. *Journal of Polymer Science Part B: Polymer Physics* **2004**, *42*, 3513–3538.
- (2) Kudaibergenov, S. E. Application of polyampholytes in emerging technologies. *Materials today: proceedings* **2022**, *71*, 31–37.
- (3) Haag, S. L.; Bernards, M. T. Polyampholyte hydrogels in biomedical applications. *Gels* **2017**, *3*, 41.
- (4) Wever, D.; Picchioni, F.; Broekhuis, A. Polymers for enhanced oil recovery: a paradigm for structure–property relationship in aqueous solution. *Progress in polymer science* 2011, 36, 1558–1628.

- (5) Mumick, P. S.; Welch, P. M.; Salazar, L. C.; McCormick, C. L. Water-soluble copolymers. 56. Structure and solvation effects of polyampholytes in drag reduction. *Macro-molecules* 1994, 27, 323–331.
- (6) Higgs, P. G.; Joanny, J.-F. Theory of polyampholyte solutions. *The Journal of chemical physics* **1991**, *94*, 1543–1554.
- (7) Baker, J. P.; Blanch, H. W.; Prausnitz, J. M. Swelling properties of acrylamide-based ampholytic hydrogels: comparison of experiment with theory. *Polymer* **1995**, *36*, 1061–1069.
- (8) He, Q.; Qiao, Y.; Medina Jimenez, C.; Hackler, R.; Martinson, A. B.; Chen, W.; Tirrell, M. V. Ion Specificity Influences on the Structure of Zwitterionic Brushes. *Macro-molecules* 2023, 56, 1945–1953.
- (9) Prusty, D.; Nap, R.; Szleifer, I.; De La Cruz, M. O. Charge regulation mechanism in end-tethered weak polyampholytes. *Soft Matter* **2020**, *16*, 8832–8847.
- (10) Kudaibergenov, S. E.; Okay, O. Behaviors of quenched polyampholytes in solution and gel state. *Polymers for Advanced Technologies* **2021**, *32*, 2639–2654.
- (11) Gao, M.; Gawel, K.; Stokke, B. T. Polyelectrolyte and antipolyelectrolyte effects in swelling of polyampholyte and polyzwitterionic charge balanced and charge offset hydrogels. *European polymer journal* **2014**, *53*, 65–74.
- (12) Lowe, A. B.; McCormick, C. L. Synthesis and solution properties of zwitterionic polymers. *Chemical reviews* **2002**, *102*, 4177–4190.
- (13) Higaki, Y.; Kobayashi, M.; Murakami, D.; Takahara, A. Anti-fouling behavior of polymer brush immobilized surfaces. *Polymer Journal* **2016**, *48*, 325–331.
- (14) Seror, J.; Merkher, Y.; Kampf, N.; Collinson, L.; Day, A. J.; Maroudas, A.; Klein, J. Articular cartilage proteoglycans as boundary lubricants: structure and frictional inter-

- action of surface-attached hyaluronan and hyaluronan–aggrecan complexes. *Biomacro-molecules* **2011**, *12*, 3432–3443.
- (15) Yang, J.; Han, Y.; Lin, J.; Zhu, Y.; Wang, F.; Deng, L.; Zhang, H.; Xu, X.; Cui, W. Ball-bearing-inspired polyampholyte-modified microspheres as bio-lubricants attenuate osteoarthritis. *Small* **2020**, *16*, 2004519.
- (16) Laschewsky, A. Structures and synthesis of zwitterionic polymers. *Polymers* **2014**, *6*, 1544–1601.
- (17) Jiang, J.; Feng, J.; Liu, H.; Hu, Y. Phase behavior of polyampholytes from charged hard-sphere chain model. *The Journal of Chemical Physics* **2006**, *124*, 144908.
- (18) Delgado, J. D.; Schlenoff, J. B. Static and dynamic solution behavior of a polyzwitterion using a Hofmeister salt series. *Macromolecules* **2017**, *50*, 4454–4464.
- (19) Shi, W. H.; Adhikari, R. S.; Asthagiri, D. N.; Marciel, A. B. Influence of charge block length on conformation and solution behavior of polyampholytes. ACS Macro Letters 2023, 12, 195–200.
- (20) Rumyantsev, A. M.; Johner, A. Salt-Added Solutions of Markov Polyampholytes: Diagram of States, Antipolyelectrolyte Effect, and Self-Coacervate Dynamics. *Macromolecules* **2023**, *56*, 5201–5216.
- (21) Madinya, J. J.; Chang, L.-W.; Perry, S. L.; Sing, C. E. Sequence-dependent self-coacervation in high charge-density polyampholytes. *Molecular Systems Design & Engineering* **2020**, *5*, 632–644.
- (22) Xiao, S.; Zhang, Y.; Shen, M.; Chen, F.; Fan, P.; Zhong, M.; Ren, B.; Yang, J.; Zheng, J. Structural dependence of salt-responsive polyzwitterionic brushes with an anti-polyelectrolyte effect. *Langmuir* **2018**, *34*, 97–105.

- (23) Li, C.; Liu, C.; Li, M.; Xu, X.; Li, S.; Qi, W.; Su, R.; Yu, J. Structures and antifouling properties of self-assembled zwitterionic peptide monolayers: effects of peptide charge distributions and divalent cations. *Biomacromolecules* **2020**, *21*, 2087–2095.
- (24) Zhu, Y.-L.; Lu, Z.-Y.; Li, Z.-W.; Sun, Z.-Y.; Liu, X. Effect of the self-assembled structures of hydrated polyzwitterionic and polyanionic brushes on their self-cleaning capabilities. *Langmuir* **2019**, *35*, 6669–6675.
- (25) Shusharina, N.; Linse, P. Oppositely charged polyelectrolytes grafted onto planar surface: Mean-field lattice theory. *The European Physical Journal E* **2001**, *6*, 147–155.
- (26) Borówko, M.; Sokołowski, S.; Staszewski, T.; Sokołowska, Z.; Ilnytskyi, J. Adsorption of ions on surfaces modified with brushes of polyampholytes. The Journal of Chemical Physics 2012, 137, 074707.
- (27) Cao, Q.; You, H. Morphologies of spherical polyampholyte brushes: Effects of counterion valence and charged monomer sequence. *Polymer* **2017**, *113*, 233–246.
- (28) Yuan, X.; Hatch, H. W.; Conrad, J. C.; Marciel, A. B.; Palmer, J. C. pH response of sequence-controlled polyampholyte brushes. *Soft Matter* **2023**, *19*, 4333–4344.
- (29) Ehtiati, K.; Moghaddam, S. Z.; Klok, H.-A.; Daugaard, A. E.; Thormann, E. Specific Counterion Effects on the Swelling Behavior of Strong Polyelectrolyte Brushes.

  \*Macromolecules\*\* 2022, 55, 5123–5130.
- (30) Murdoch, T. J.; Willott, J. D.; de Vos, W. M.; Nelson, A.; Prescott, S. W.; Wanless, E. J.; Webber, G. B. Influence of anion hydrophilicity on the conformation of a hydrophobic weak polyelectrolyte brush. *Macromolecules* 2016, 49, 9605–9617.
- (31) Gregory, K. P.; Elliott, G. R.; Robertson, H.; Kumar, A.; Wanless, E. J.; Webber, G. B.; Craig, V. S.; Andersson, G. G.; Page, A. J. Understanding specific ion effects and the Hofmeister series. *Physical Chemistry Chemical Physics* 2022, 24, 12682–12718.

- (32) Parsons, D. F.; Boström, M.; Nostro, P. L.; Ninham, B. W. Hofmeister effects: interplay of hydration, nonelectrostatic potentials, and ion size. *Physical Chemistry Chemical Physics* **2011**, *13*, 12352–12367.
- (33) Prusty, D.; Gallegos, A.; Wu, J. Unveiling the Role of Electrostatic Forces on Attraction between Opposing Polyelectrolyte Brushes. *Langmuir* **2024**, *40*, 2064–2078, PMID: 38236763.
- (34) Jiang, T.; Wu, J. Self-organization of multivalent counterions in polyelectrolyte brushes.

  The Journal of Chemical Physics 2008, 129, 084903.
- (35) Jiang, T.; Li, Z.; Wu, J. Structure and Swelling of Grafted Polyelectrolytes: Predictions from a Nonlocal Density Functional Theory. *Macromolecules* **2007**, *40*, 334–343.
- (36) Jiang, T.; Wu, J. Ionic effects in collapse of polyelectrolyte brushes. *The Journal of Physical Chemistry B* **2008**, *112*, 7713–7720.
- (37) Wong, J. E.; Zastrow, H.; Jaeger, W.; von Klitzing, R. Specific ion versus electrostatic effects on the construction of polyelectrolyte multilayers. *Langmuir* **2009**, *25*, 14061–14070.
- (38) Li, Z.; Wu, J. Density functional theory for polyelectrolytes near oppositely charged surfaces. *Physical review letters* **2006**, *96*, 048302.
- (39) Li, Z.; Wu, J. Density functional theory for planar electric double layers: Closing the gap between simple and polyelectrolytes. *The Journal of Physical Chemistry B* **2006**, 110, 7473–7484.
- (40) Wu, J. Understanding the Electric Double-Layer Structure, Capacitance, and Charging Dynamics. *Chemical Reviews* **2022**, *122*, 10821–10859.
- (41) Shusharina, N.; Linse, P. Polyelectrolyte brushes with specific charge distribution: Mean-field lattice theory. *The European Physical Journal E* **2001**, 4, 399–402.

- (42) Gallegos, A.; Müller, M.; Wu, J. Single-chain simulation of Ising density functional theory for weak polyelectrolytes. *The Journal of Chemical Physics* **2023**, *159*, 214902.
- (43) Wang, T.; Kou, R.; Liu, H.; Liu, L.; Zhang, G.; Liu, G. Anion specificity of polyzwitterionic brushes with different carbon spacer lengths and its application for controlling protein adsorption. *Langmuir* **2016**, *32*, 2698–2707.
- (44) Tan, H.-G.; Guo, L.-D.; Qian, H.-Y.; Liu, L.-X.; Hao, Q.-H.; Miao, B. Size Effect of Multivalent Counterions on Polyelectrolyte Brushes in Different Polar Solvents. *Macro-molecules* 2023, 56, 9312–9323.